University of Vermont

ScholarWorks @ UVM

3-1-2015

The use of CMIP5 data to simulate climate change impacts on flow regime within the Lake Champlain Basin

Ibrahim Nourein Mohammed
University of Vermont

Arne Bomblies
University of Vermont

Beverley C. Wemple
University of Vermont

Follow this and additional works at: https://scholarworks.uvm.edu/casfac

Part of the Climate Commons

Recommended Citation

The use of CMIP5 data to simulate climate change impacts on flow regime within the Lake Champlain Basin

Ibrahim Nourein Mohammed [a,*], Arne Bomblies [a,b], Beverley C. Wemple [a,c]

[a] University of Vermont, EPSCoR, 23 Mansfield Ave, Room 208A, Burlington, VT 05401, USA
[b] University of Vermont, Department of Civil and Environmental Engineering, 221 Votey Hall, Burlington, VT 05405, USA
[c] University of Vermont, Department of Geography, 208 Old Mill, Burlington, VT 05405, USA

ARTICLE INFO

ABSTRACT

Study region: Lake Champlain Basin, northwestern New England, USA.
Study focus: Our study uses regional hydrologic analyses and modeling to examine alternative possibilities that might emerge in the Lake Champlain Basin streamflow regime for various climate scenarios. Climate data as well as spatial data were processed to calibrate the Regional Hydro-Ecological Simulation System (RHESSys) model runoff simulations. The 21st century runoff simulations were obtained by driving the RHESSys model with climate data from the Coupled Model Intercomparison Project phase 5 (CMIP5) for representative concentration pathways RCP 4.5 and 8.5.
New hydrological insights for the region: Our analyses suggest that most of CMIP5 ensembles fail to capture both the trends and variability observed in historical precipitation when run in hindcast. This raises concerns of using such products in driving hydrologic models for the purpose of obtaining reliable runoff projections that can aid researchers in regional planning. A subset of five climate models among the CMIP5 ensembles have shown statistically significant trends in precipitation, but the magnitude of these trends is not adequately representative of those seen in observed annual precipitation. Adjusted precipitation forecasts project a streamflow regime described by an increase of about 30% in seven-day maximum flow, a four days increase in flooded days, a three orders of magnitude increase in base flow index, and a 60% increase in runoff predictability (Colwell index).

* Corresponding author. Tel.: +1 802 656 7351; fax: +1 802 656 2950.
E-mail addresses: Ibrahim.mohammed@uvm.edu (I.N. Mohammed), abomblie@uvm.edu (A. Bomblies), Beverley.Wemple@uvm.edu (B.C. Wemple).

1. Introduction

Over the past several decades, temperature and precipitation have increased significantly in the northeastern United States (Hayhoe et al., 2007, 2008; Huntington et al., 2009; Melillo et al., 2014). Understanding the impacts of these climatic changes on watershed hydrology is important for human society and ecological processes. However, the observed climate trends show significant spatial variability within New England in addition to pronounced seasonality (Hayhoe et al., 2008). Recent dissemination of downscaled Global Circulation Model (GCM) data has made such regional analysis tractable. For example, statistically downscaled data products such as the Coupled Model Intercomparison Project (CMIP5) multi-model ensemble and its predecessors are commonly applied as drivers of hydrology models (Meehl et al., 2007; Taylor et al., 2011; Meehl et al., 2014). Such downscaled data have great potential to aid researchers, resource managers, and other policy makers in the assessment of climate change impacts on water and the environment. However, at least two studies have documented poor correlation between precipitation obtained from such downscaled climate model products and observations (Stephens et al., 2010; van Haren et al., 2013), therefore the applicability of CMIP5 precipitation data for regional hydrological impacts analysis must be validated.

Changes in streamflow regime in the northeastern United States have been examined in multiple studies using historical datasets (Hartley and Dingman, 1993; Hodgkins et al., 2003, 2005; Hodgkins and Dudley, 2005, 2006; Campbell et al., 2011). These works summarized the observed northeastern streamflow regime change as timing shift toward earlier spring flow and a more uniform distribution of flow throughout the snowmelt period (i.e., March streamflows have increased, while May flows have declined). However, summer baseflow increased in undammed New England rivers during the latter half of the twentieth century (Hodgkins and Dudley, 2011).

Potential impacts of climatic changes on aquatic ecosystems species, nutrient delivery, temperatures and hydrology have been discussed for different regions of the United States (Melack et al., 1997; Hauer et al., 1997; Mulholland et al., 1997; Moore et al., 1997; Stone et al., 2001). Natural flow regime plays a major role in sustaining native biodiversity and ecosystem integrity in rivers (Poff et al., 1997). Streamflow regime alteration may also affect aquatic organisms, sediment movement and floodplain interactions (Gibson et al., 2005). Characterization of flow regime has been examined via metrics that describe the magnitude, frequency, duration, timing and rate of change for streamflow (Poff, 1996; Poff et al., 1997; Puckridge et al., 1998). These streamflow metrics are useful determinants of ecological process regulation in river ecosystems. Numerous similar streamflow regime metrics have been compiled (Richter et al., 1996; Puckridge et al., 1998; Snelder and Biggs, 2002).

The Lake Champlain Basin is a multi-state and bi-national watershed (Vermont, New York and Québec) with a drainage area of about 21,000 km^2 (Stager and Thill, 2010) and serves as a major source of ecosystem services and economic inputs to the northeastern United States. Predicted 21st century climatic changes are expected to impact a range of environmental processes in the Basin and therefore raise concerns about hydrological, ecological as well as political conditions (Stager and Thill, 2010). Therefore, an evaluation of climate change impacts on regional hydrology would greatly benefit policymakers and other stakeholders. In this study, we examine the reliability of the CMIP5 ensemble of simulations in performing regional hydrological impacts analysis in northwestern New England. We also discuss the uncertainty associated with climate change impacts on a Vermont watershed flow regime. We perform such an assessment in the Mad River watershed of Vermont, and subsequently predict future flow regime for the Mad River using the downscaled climate data using metrics that are useful to policymakers and ecologists.

2. Methods

2.1. Study area

The Mad River near Moretown is a 360 km^2 tributary watershed of the Winooski River (HUC 02010003) within the Vermont portion of the Lake Champlain basin (Fig. 1). This watershed is a representative study area for examining the impacts of climate change on streamflow regime since the mixed forested, agricultural and village center land covers are typical of the Vermont landscape.
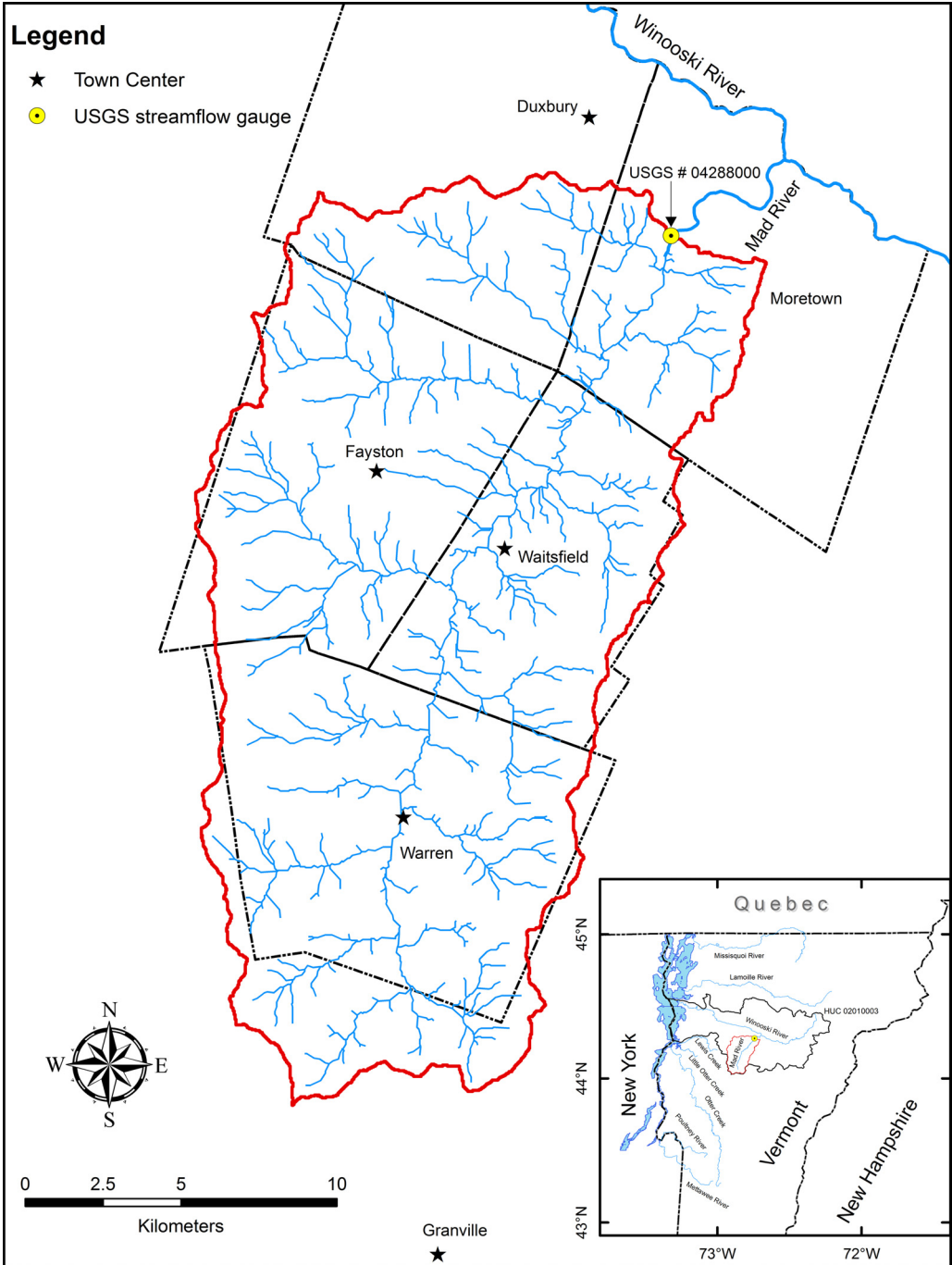
Fig. 1. Mad River near Moretown watershed (USGS # 04288000) is located within the Winooski basin (HUC 02010003). The watershed drainage area is about 360 km². The headwater of the Mad River is Granville Notch Falls. Mad River drains into the Winooski River which in turn drains into Lake Champlain.

The watershed is mainly forested with urbanized town centers (about 4% of watershed area) and agricultural lands (about 8% of watershed area) found mainly on the valley floor.

A long monitoring streamflow data record is available for the Mad River watershed at its outlet. The watershed outlet (United States Geological Survey (USGS) streamflow gauge # 04288000) is located at 44°16′38″ North and 72°44′35″ West (referenced to the North American Datum (NAD) of 1927) within the Washington County, Vermont. The gauge altitude is 170 m above sea level referenced to the National Geodetic Vertical Datum (NGVD) of 1929. The Mad River flows north toward the Winooski River, which flows to Lake Champlain. Lake Champlain is drained by the Richelieu River to the north and is situated within the St. Lawrence River drainage. The streamflow record at the Mad River gauge begins in October 1928. Streamflow data for this work was retrieved from the USGS portal (http://waterdata.usgs.gov/nwis/dv/?site_no=04288000&agency_cd=USGS&referred_module=sw) accessed on 4 February 2014. Mean annual runoff (Q) measured at the outlet of the study watershed during the period 1950–2013 (water years) is 714 mm. April is the highest yield month at the watershed outlet with monthly median runoff of 160 mm, and in drier months, occasional fluctuations at low flow have occurred. Mean annual precipitation ($\overline{Pcp}$) on the study watershed is 1235 mm. Table 1 shows the annual mean precipitation, runoff and evapotranspiration ($\overline{E}$) for the years 1920–2010 over the study watershed. The annual average evapotranspiration was calculated using mass balance ($\overline{E} = \overline{Pcp} - \overline{Q}$).

2.2. Spatial data

A digital elevation model (DEM) with 30 m grid resolution for the study area was obtained from the National Elevation Dataset (NED) portal (http://seamless.usgs.gov/website/seamless/viewer.htm) and was used to derive slope and aspect grids for the model input. Fig. 2, panel (a) shows the topography of our study watershed, which ranges from 170 to 1240 m above sea level with a mean value of 491 m.

Land use and vegetation data were obtained from the National Land Cover Dataset (NLCD 2006) (http://gisdata.usgs.net/website/MRLC/viewer.htm). We grouped vegetation and land use for our study watershed into eight categories: coniferous forest, deciduous forest, mixed forest, grassland, no vegetation, shrub, agriculture and urban. The forest cover dominates about 87% of the watershed area (52% deciduous, 23% mixed, and 12% conifer forests). There are a few agricultural lands and small urban areas within valleys and scattered over the watershed area (Fig. 2, panel b).

The watershed surface soil texture map was obtained from the Natural Resources Conservation Service County Soil Survey Data dataset through the Vermont Center for Geographic Information Gateway (http://vcgi.vermont.gov/). County soil data for the Washington, Addison and Chittenden counties were obtained to compile our watershed soil texture map. The watershed soil texture is mainly sandy clay loam (approximately 80% of the watershed area) which has 34% clay content. The mean soil depth at the valley floor is approximately 1.5 m.

2.3. Climate data

Daily precipitation (Pcp), minimum and maximum air temperatures (T_{min} and T_{max}), and wind speed (w) data were obtained from the Santa Clara University portal (http://www.engr.scu. edu/ emaurer/data.shtml) (Maurer et al., 2002). The data is at daily and 1/8th degree resolutions for the period 1 January 1949 to 31 December 2010, and constitutes the historical climate data set for our

Table 1
Mad River near Moretown, Vermont (USGS # 04288000) annual water balance estimates (1950–2010). Precipitation (Pcp) from Maurer et al. (2002), Runoff (Q) from the USGS national water information system (http://waterdata.usgs.gov/nwis) gauge number 04288000. Mean annual evapotranspiration estimated from mass balance.

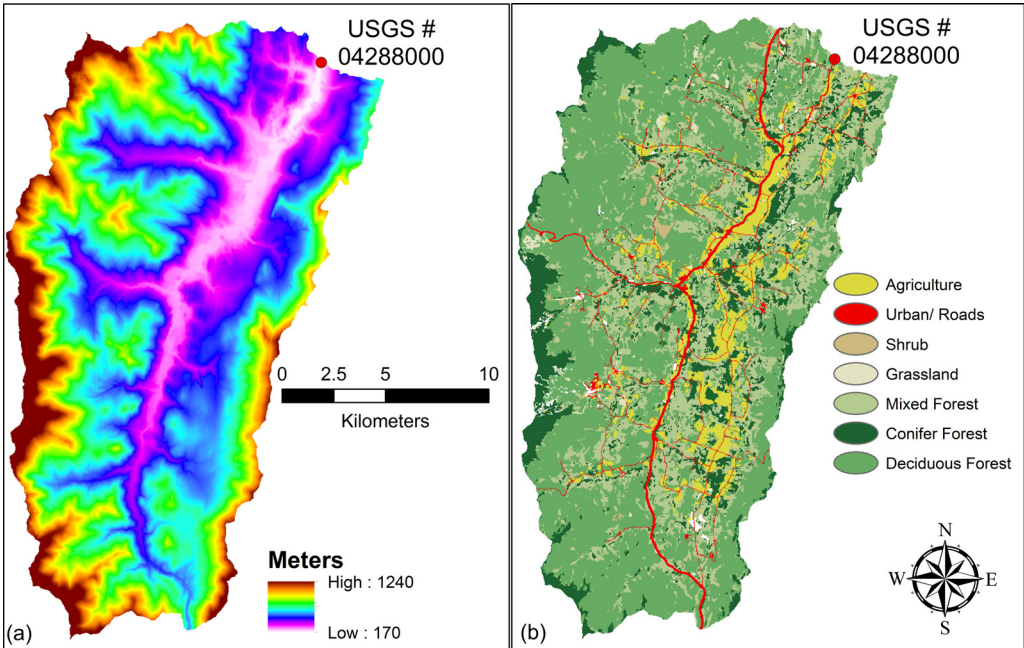| Variable	Minimum	25th percentile	Median	Mean	75th percentile	Max
Pcp (mm)	851	1091	1198	1235	1361	1805
Q (mm)	332	579	671	682	786	1074
$\overline{E}$ (mm)				553		

Fig. 2. Spatial input data. (a) Digital elevation model (DEM) (30 m grid size) and (b) land cover. Land cover data are from the NLCD 2006 dataset.

study. The climatic seasonal variation for our study watershed is shown in Fig. 3. July is the hottest month of the year with average daily maximum and minimum air temperatures of 24 and 13 °C respectively.

Output data from two scenarios of Representative Concentration Pathways (*RCP 4.5* and *8.5*) simulations of GCM output data (daily precipitation, minimum and maximum air temperatures) were obtained from the Coupled Model Intercomparison Project phase 5 (CMIP5) multi-model ensemble (Taylor et al., 2011). The gridded datasets are all at 1/8th degree resolution, and aggregate metrics for precipitation (*Pcp*) and air temperatures (T_{min} and T_{max}) were calculated for the eight grid cells spanning the Mad River watershed.

Downscaled model inputs selected were the bias correction constructed analogs method (BCCA) products discussed by Maurer et al. (2010). Full details about the climate scenario data are in Brekke et al. (2013). For this work, we utilized the gridded bias-corrected climate scenarios data for the 2006–2100 time period as well as the retrospective climate data for 1951–2005 time period (further details on climate models can be found at Appendix A).

A visual assessment of the CMIP5 projection ensembles hindcast data when compared with observed historic precipitation (Maurer et al., 2002) suggests that the CMIP5 model ensembles have poorly captured the variability and trends historically observed. Fig. 4 shows the annual observed precipitation time series over the study watershed during 1951–2005 water years along with the twenty-one CMIP ensembles when run on a hindcast mode.

Figs. 5 and 6 show annual precipitation and annual air temperatures (minimum and maximum), respectively, aggregated over our study watershed from the CMIP5 subset ensembles under the *RCP 8.5* scenario. There is a large difference in the slope between historical and future precipitation projections.

2.4. RHESSys model description

The Regional Hydro-Ecologic Simulation System (RHESSys) model described by Band et al. (1993, 1996) and Tague and Band (2001, 2004) is a GIS-based, hydro-ecological modeling framework designed
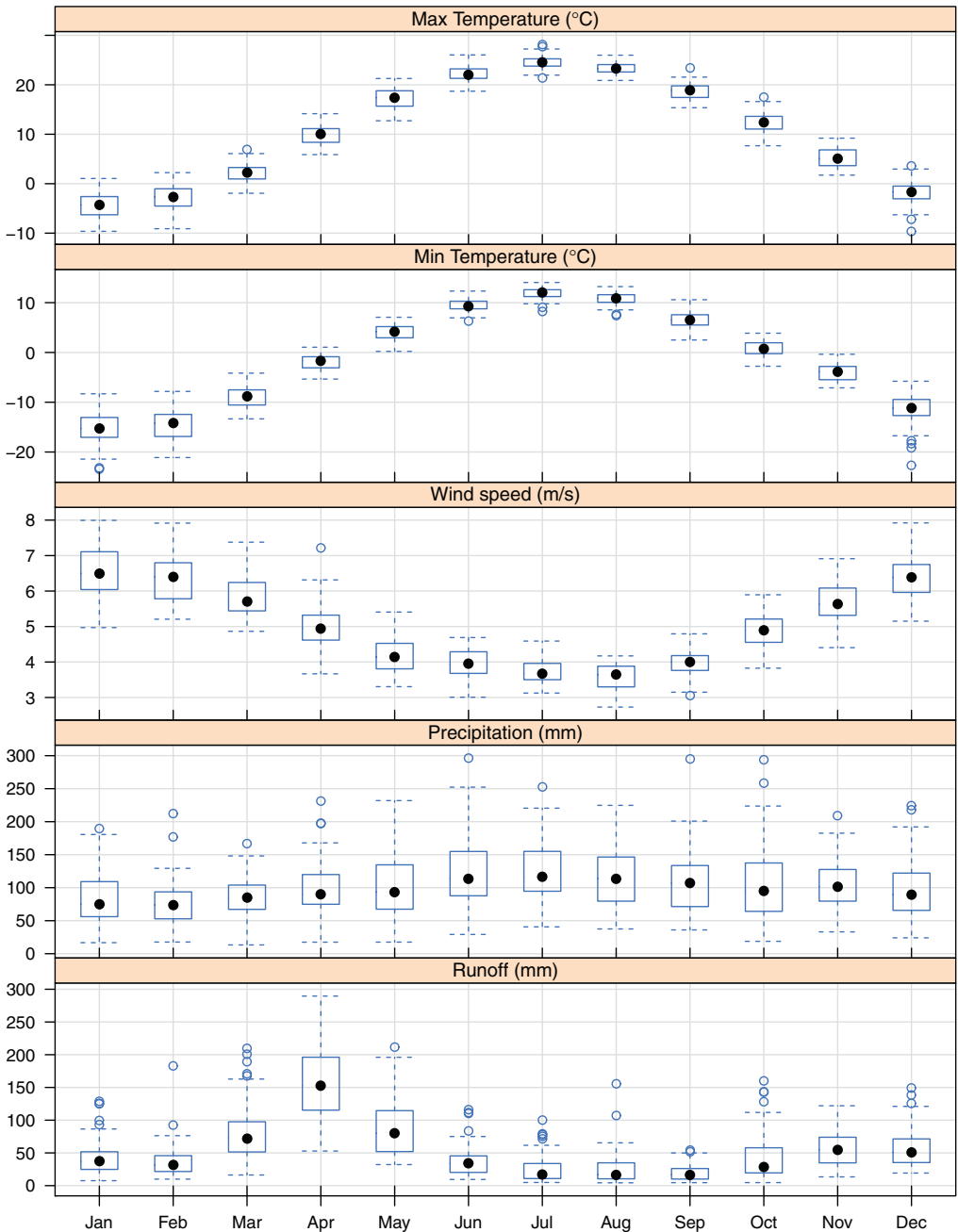
Fig. 3. Historic climate input data over the study watershed and measured runoff at the Mad River near Moretown watershed outlet (USGS gauge # 04288000) during 1949–2010. Boxplots of monthly averages of minimum, maximum air temperatures and wind speed. Boxplots of precipitation and runoff amounts summed monthly. Climate data obtained from Maurer et al. (2002).
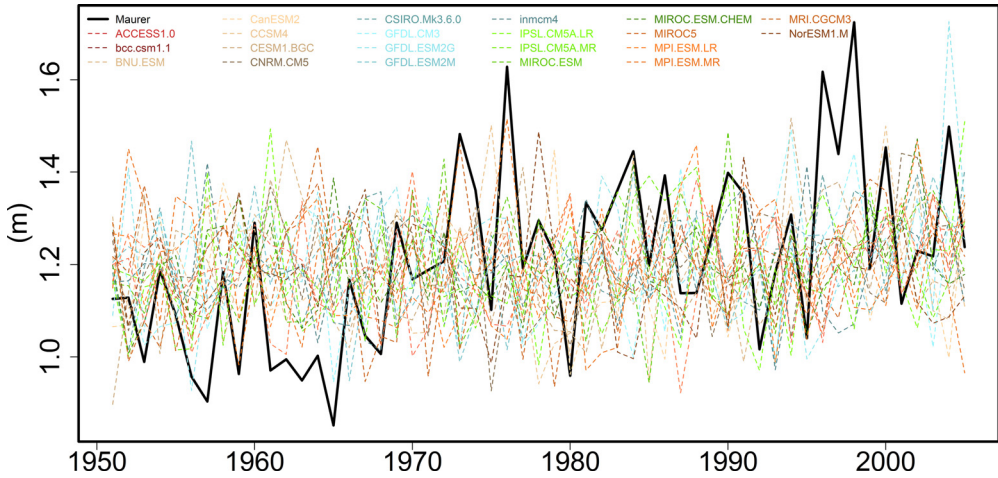
Fig. 4. Annual historic precipitation aggregated over the Mad River near Moretown watershed (USGS gauge # 04288000) during 1951–2005 water years. Observed data obtained from Maurer et al. (2002) depicted as solid black line (Maurer), while climate data of twenty one climate models (run on hindcast) were obtained from the Coupled Model Intercomparison Project phase 5 (CMIP5) ensembles (http://gdo-dcp.ucllnl.org/downscaled_cmip_projections/dcpInterface.html).

Fig. 5. Annual precipitation aggregated over the Mad River near Moretown watershed (USGS gauge # 04288000). Historical climate data obtained from Maurer et al. (2002), while scenario (*RCP 8.5*) climate data of five climate models were obtained from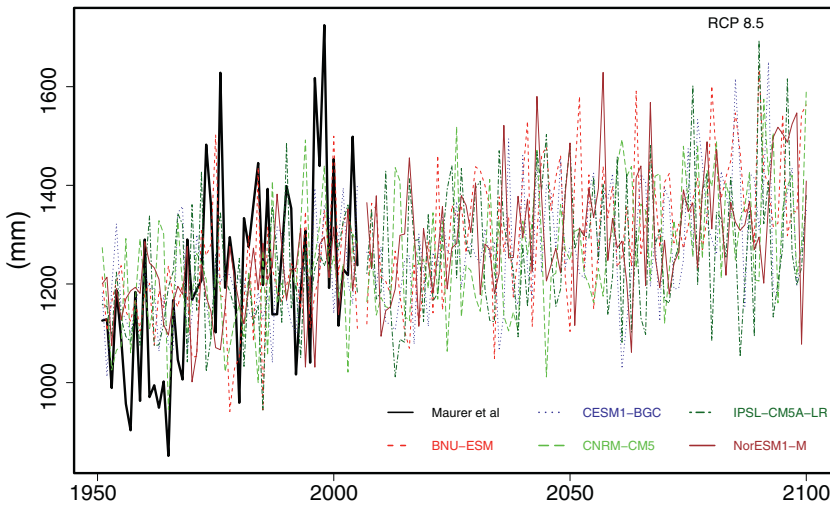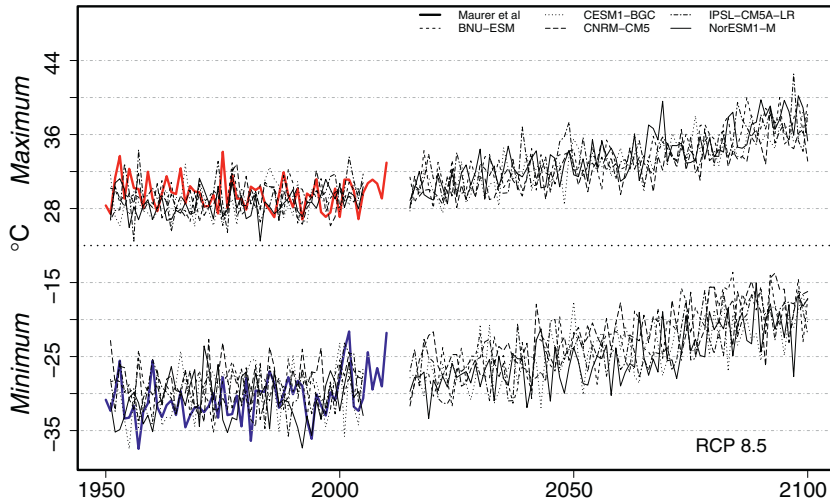 the Coupled Model Intercomparison Project phase 5 (CMIP5) ensembles (http://gdo-dcp.ucllnl.org/downscaled_cmip_projections/dcpInterface.html).

to simulate carbon, water and nutrient fluxes. RHESSys combines both a set of physically based process models and a methodology for partitioning and parameterizing the landscape over spatially variable terrain ranging from ten meters to hundreds of kilometers. The version of RHESSys used for this work (5.14.4) includes both surface and subsurface storage routing and a deep groundwater store (Tague et al., 2008). The RHESSys model is able to simulate interactions between carbon, water and nutrient fluxes and climate patterns within a mountainous environment. Water is explicitly routed between spatial patches, representing spatial heterogeneity in soil moisture and lateral water flux to the stream. The RHESSys hydrologic process models have been adapted from several pre-existing

Fig. 6. Annual minimum and maximum air temperature aggregated over the Mad River near Moretown watershed (USGS gauge # 04288000). Historical climate data obtained from Maurer et al. (2002), while scenario (*RCP 8.5*) climate data of five climate models were obtained from the Coupled Model Intercomparison Project phase 5 (CMIP5) ensembles (http://gdo-dcp.ucllnl.org/downscaled_cmip_projections/dcpInterface.html). Maurer et al. data are depicted in red and blue colors for maximum and minimum air temperatures respectively.

models and they include snow accumulation and melt, interception, infiltration, transpiration, soil and litter interception, evaporation and shallow and deep groundwater subsurface lateral flow. Most processes are run at a daily time step.

For this work, we used the routing approach adapted from the Distributed Hydrology Soil and Vegetation Model (DHSVM) (Wigmosta et al., 1994) to route the water laterally. The DHSVM routing model simulates saturated subsurface interflow and overland flow via pixel-by-pixel basis connectivity. An important modification from the grid-based routing of DHSVM is the ability of RHESSys to route water between arbitrarily shaped surface elements. This allows greater flexibility in defining surface patches and varying shape and density of surface tessellation. Then a reasonable approximation of reality in simulating lateral moisture routing at the level of spatial data resolution employed is achieved.

RHESSys partitions the landscape into distributed elements hierarchically organized into *basin* (watershed), *zone*, *hillslope*, *patch* and *stratum*. In this work, *zones* representing climate information have been partitioned following the 1/8th degree climate grid from Maurer et al. (2002). There are eight different zones spanning our study watershed. *Hillslopes* were generated using the watershed analysis routine (*r.watershed*) in GRASS (GRASS Development Core Team, 2012) with contributing area threshold of 21,600 m^2 resulting in 16,560 hillslopes. We obtained the stream network contributing area threshold objectively from a stream drop test following theory described in Tarboton et al. (1991, 1992). Each hillslope was treated as a single model element (i.e., *patch*). *Stratum* is used for canopy information and inherits the *patch* spatial setting (i.e., *hillslope* in this work).

RHESSys uses the Mountain Microclimate Simulator (MTN-CLIM) model (Running et al., 1987) to obtain spatially variable climate inputs. Daily climate data of minimum and maximum air temperature as well as precipitation drive RHESSys flux estimates. The MTN-CLIM model simulates radiation, partitioning of rain and snow, saturation vapor pressure, and relative humidity. MTN-CLIM extrapolates meteorological variables from the point of measurements to the modeling unit of interest (*hillslope*) making corrections for differences in elevation, slope and aspect between the point of measurements and targets (*hillslopes*). Lapse rates used in this work to adjust air temperatures and dewpoint spatially are 0.01 and 0.0015 °C/m, respectively.

Canopy heights and species specific vegetation parameters (Myers and Edminster, 1972; Kaufmann and Troendle, 1981; Ryan, 1990; White et al., 2000; Rueth and Baron, 2002) are available as standard

Table 2
Streamflow regime variables used to examine climate changes impacts.

Variable name	Symbol	Definition	Streamflow classification
Daily mean discharge	QMEAN	Average daily flow over a water year	Static basin descriptor
High flow disturbance	Q1.67	Flow of magnitude exceeding a return interval of 1.67 years based on a log-normal distribution	High flow disturbance
Flood duration	FLDDUR	The average number of days per year when flow equals or exceeds Q1.67	
7 day maximum flow	7QMAX	The average annual maxima of 7 day means of daily mean streamflow	
Base flow index	BFI	The ratio of the annual lowest daily flow to the average daily flow multiplied by 100 during a water year	Low flow disturbance
7 day minimum flow	7QMIN	The average annual minima of 7 day means of daily mean streamflow	
Coefficient of variation	DAYCV	The ratio of the standard deviation of daily flows to the average of daily flows multiplied by 100 during a water year	Flow variability and predictability
Flow reversal	R	The average number of daily flow reversals per year	
Colwell index of Predictability	P	Predictability of flow using an index	
Colwell index of Constancy	C	developed by Colwell (1974) which is	
Colwell index of Contingency	M	based on information theory	

RHESSys libraries. The six vegetation categories grouped for the study watershed were linked with vegetation parameters from RHESSys libraries.

Initial leaf area index (LAI) values at the *hillslope* level for our study watershed were found by reclassifying specific vegetation classes with LAI values. LAI values for each vegetation class used for reclassification were obtained from White et al. (2014) and suggested literature over the study region (Dingman, 2002, Table 7–5). The aggregate average LAI over the study watershed is about 4.6.

RHESSys uses many parameters to describe typical soil, vegetation and land use characteristics. Literature-based estimates have been used to compile parameters for common vegetation and soil types. Calibrated parameters within RHESSys are (1) the decay of hydraulic conductivity with depth (m), (2) saturated soil hydraulic conductivity at the surface (k), (3) the fraction of recharge that bypasses the shallow subsurface flow system to deeper groundwater storage ($gw1$), and (4) the drainage rate of deeper groundwater store ($gw2$).

2.5. Flow regime

In this paper, we examine three streamflow classes and how they change with climate at the Mad River near Moretown streamflow gauge (watershed outlet). The streamflow classes studied are high flow disturbance, low flow disturbance and flow variability and predictability (Table 2).

High flow disturbance streamflow metrics include three streamflow variables: a high flow disturbance variable ($Q1.67$), a flood duration ($FLDDUR$) variable, and a seven-day maximum flow ($7QMAX$) variable. Dunne and Leopold (1978) define bankfull stage as "the stage that corresponds to the discharge at which channel maintenance is the most effective, that is, the discharge at which moving sediment, forming or removing bars, forming or changing bends and meanders, and generally doing

work results in the average morphologic characteristics of channel." Wolman and Miller (1960) concluded that the bankfull stage is the most effective or is the dominant channel forming flow. There is a wide agreement that on average a bankfull flow has an average recurrence interval of 1.5 years, however Poff (1996) and Chinnayakanahalli et al. (2011) cite that a flow with a 1.67 year return interval is often recognized as bankfull flow. The *Q1.67* flow is defined as a flow of magnitude exceeding a return interval of 1.67 years based on fitting a log-normal probability distribution to the annual maximum daily flow series then selecting the value that has a probability of exceedance of 1/1.67 (Dunne and Leopold, 1978). Historical streamflow data (1955–2013 water years) at the study watershed gauge suggest that *Q1.67* for the study gauge is about 24 millimeter per day (3,587 cfs). Flood duration (*FLD-DUR*) is usually calculated as the average number of days per year when flow equals or exceeds *Q1.67* flow. For the historical streamflow period studied, the mean flood duration for the study watershed using a return flow of 24 mm/day is less than one day.

Since the Mad River watershed is flashy, estimating the magnitude of daily return flow that we can use in calculating flood duration periods is quite challenging (floods last only several hours). The National Weather Service (NWS) flood stage guidelines at our watershed (http://water.weather.gov/ahps2/hydrograph.php?wfo=btv&gage=moov1), accessed on 26 February 2014, indicate that nine feet is the threshold stage for flood warning. We thus take the Mad River near Moretown streamflow gauge bankfull stage as nine feet. We extracted all the days when stage at our watershed was equal to or exceeded 9 *feet* from the historical instantaneous crests record during 1927–2013 provided by the USGS. The instantaneous flood peak flows vary from four to 166 mm/day (i.e., 530–24,300 cfs). We examined the daily runoff values at these flooded days. We found that the daily runoff at these flooded days varies from about 1 to 44 mm/day (i.e., 160–6,140 cfs) with 25th percentile at 15 mm/day (2,175 cfs) and 50th percentile at 24 mm/day (3,575 cfs). Mapping historical crest data on daily flow data is more realistic in terms of capturing flood duration rather than just relying on the *Q1.67* discussed earlier. The threshold used to calculate flood duration periods for this work was set as 15 mm/day (25th percentile).

A simple way to depict a distribution is to examine a histogram. A histogram counts the number of occurrences within predefined bins. However, identifying modes from the histogram requires visual interpretation and is somewhat subjective because of the choice of bin width. Silverman (1986) presented nonparametric density estimation methods that can depict the distribution of data more generally and objectively. Kernel methods are popular nonparametric approaches that we have used here to show different flood scenarios. The kernel methods are most sensitive to the selection of bandwidth (h). There are multiple methods that give estimates for the bandwidth (h) (Silverman, 1986; Sheather and Jones, 1991; Scott, 1992). Here we used the *Sheather and Jones* method implemented by the *R* statistical software package to select bandwidth (h) (R Development Core Team, 2014) and a Gaussian function for the kernel.

Seven-day maximum flow (*7QMAX*) is the average across years of 7-day maximum streamflow. For each year in the period of record, the maximum 7-day mean is found from the daily mean streamflow and the maximum is the 7-day maximum flow for that year. A *7QMAX* is the average of those yearly 7-day maximum values and for the historical data; it is about 10 millimeters per day (1,513 cfs).

Low flow disturbance streamflow metrics include a baseflow index for a measure of changes in base flow (*BFI*) variable and a 7-day minimum (*7QMIN*) variable. Baseflow index (*BFI*) is the ratio of the annual lowest daily flow to the average flow multiplied by 100. *BFI* is a low flow variable that indexes flow stability and susceptibility to drying. Historical streamflow data suggests that the median of *BFI* at the study gauge is about 9%. Seven-day minimum flow (*7QMIN*) variable is the average across years of 7-day minimum streamflow. For each year in the period of record, the minimum 7-day mean is found from the daily mean streamflow and the minimum is the 7-day minimum flow for that year. A *7QMIN* is the average of those yearly 7-day minimum values and for the historical data; it is about one millimeter per day (199 cfs).

Flow variability and predictability streamflow metrics include a coefficient of variation (*DAYCV*) variable, a flow reversal (*R*) variable and three flow variables defining the Colwell index which are Predictability, Constancy and Contingency (Colwell, 1974). Flow reversal events are often related to physical disturbance in stream ecology (Resh et al., 1988). Streamflow variability exerts control over many important structural attributes in streams (e.g., habitat volume, current velocity, channel

geomorphology, and substratum stability). Temporal patterns of streamflow are important in the fluctuating physical and biological environment of rivers (Lazzaro et al., 2013).

Coefficient of variation (*DAYCV*) is the standard deviation of daily flows divided by the average of daily flows multiplied by 100 during a year. The *DAYCV* describes overall flow variability without considering the temporal sequence of flow variation. Historical data suggests that the median of *DAYCV* at the study watershed is about 137%, which suggests a high rate of streamflow change (flashiness).

Flow reversals (*R*) are defined from the daily mean streamflow as days when the trend (increasing or decreasing) from the previous days is reversed. Historical streamflow data from the study gauge gives the median of *R* as about 125 days.

Flow predictability metrics were developed (*Colwell's* indices, Colwell, 1974) to assess biologically relevant measures of flow variability. The principal value of the Colwell index used in our work is for comparison of the uncertainty of the variable river environment projected in future. The Colwell index is also useful for the association of natural variation in flow regime with aquatic macroinvertebrate taxa richness and composition within the ecological community (Poff and Ward, 1989; Chinnayakanahalli et al., 2011). Stream ecologists are often interested in this theory because of the great temporal variability within and between river ecosystem environments. Colwell (1974) procedure is analogous to autocorrelation analysis and to some aspects of harmonic analysis. The *Colwell's* predictability (*P*) is the sum of constancy (*C*) and contingency (*M*). Constancy (*C*) is a measure of temporal invariance, and contingency (*M*) is a measure of periodicity. Constancy is defined similar to predictability, except that seasonal variability across periods is disregarded. Contingency is defined as the degree to which time period and value group are dependent on each other. The *P*, *C*, and *M* are scaled to range from 0 to 1 (further details on Colwell index are presented at Appendix B).

Calculation of *Colwell's* indices requires that streamflow values be binned into discrete groups. As with all information measures absolute values are dependent on this binning, but a consistent binning allows relative comparisons. Following Gordon et al. (2004) and Chinnayakanahalli et al. (2011), we used 7 bins (<0.5 μ, 1.0 μ, 1.5 μ, 2.5 μ, 3.0 μ, >3.0 μ), where μ is equal to the mean of daily streamflow values, to define groups for each month. We used twelve months to represent the seasonal cycle and counted the number of occurrences of daily streamflow values in states defined by groups (bins) and periods (months). Analysis of the Mad River watershed historical streamflow data (1955–2013 water years) using these metrics indicates that the flow has a low predictability (*P* ≈ 0.25) The Constancy (*C*) at the observed historical predictability is 0.23. Fish species observed at the Mad River mouth (i.e., warm water fish habitat) are Brook trout, Longnose dace, and Slimy sculpin. We infer that the observed low Colwell's predictability calculated is suitable to maintain the above-mentioned species.
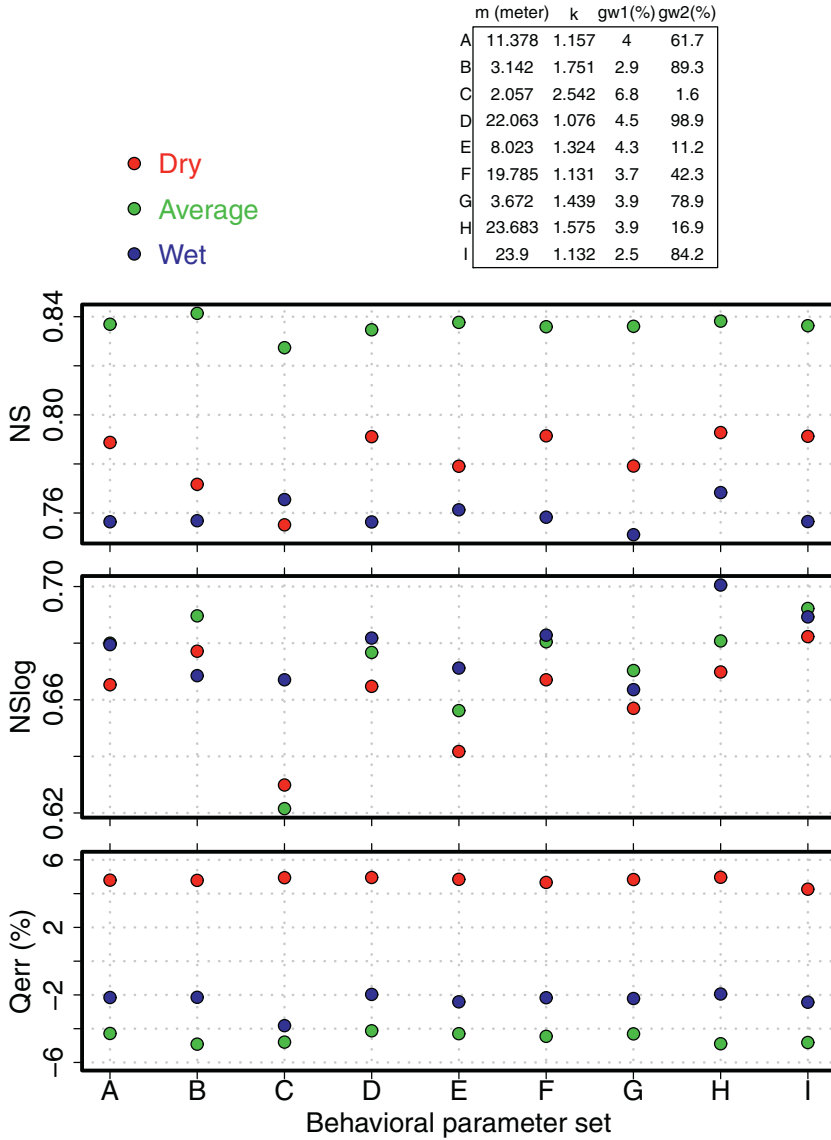
3. Results

3.1. Model calibration and verification

In this work, the model was calibrated to daily streamflows at the watershed outlet during three different water years (wet, average and dry) in order to assess model performance over a range of climatic conditions. The wet water year selected for model calibration has annual precipitation of 1445 mm. Monte Carlo simulation was used to generate 5500 sample parameter sets from independent uniform distributions over the feasible parameter ranges determined from the literature ranges for *m*, *k*, *gw1*, and *gw2* parameters. Each sample parameter set was used as an input to the model, and model performance was assessed using the Nash–Sutcliffe efficiency metric on daily flows (*NS*), Nash–Sutcliffe efficiency metric on log daily flows (*NSlog*) and total annual flow error (*Qerr*). We repeated this step for the remaining selected water years (average and dry) and results were shown in Fig. 7 (average water year). We note that model results were more sensitive to changes in values of *gw1* and *gw2* parameters than to changes in the other parameters. The saturated soil hydraulic conductivity at the surface (*k*) parameter depicted in Fig. 7 is a multiplier of hydraulic conductivity at the surface for both soil texture types used in the watershed soil texture map (sandyclayloam soil hydraulic conductivity at the surface used was about 0.544 m/day, while clay hydraulic conductivity at the surface used was about 0.111 m/day).
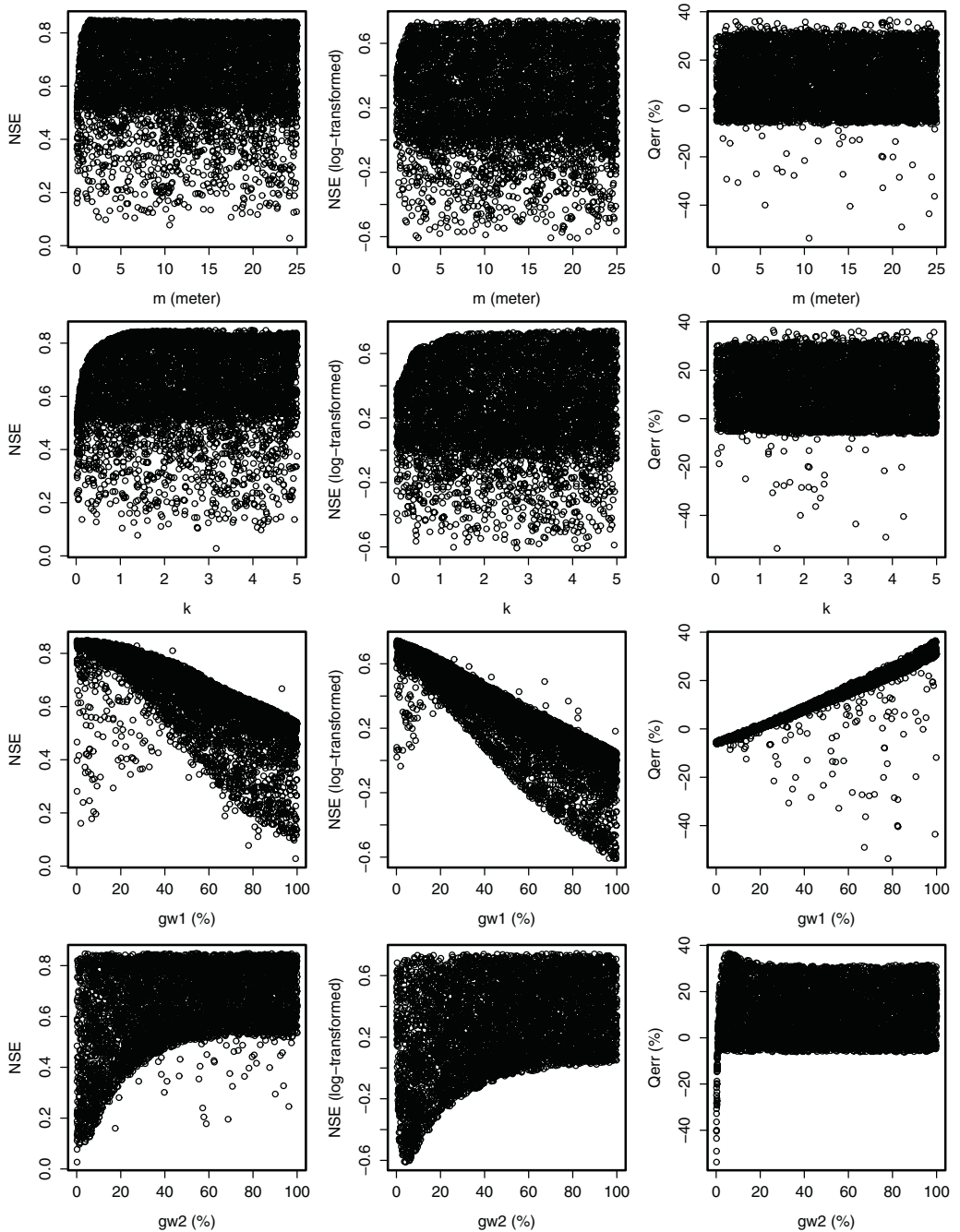
Fig. 7. Five thousand and five hundred Monte Carlo simulation sample parameter sets over the literature parameter ranges for RHESSys calibration parameters (*m*, *k*, *gw1*, and *gw2*). Nash–Sutcliffe efficiency metric on daily flows (*NS*), Nash–Sutcliffe efficiency metric on log daily flows (*NSlog-transformed*) and annual flow error (*Qerr*) metrics were used to pick a reasonable set of RHESSys calibration parameters. An average water year observed runoff record was used for calibration.

	m (meter)	k	gw1(%)	gw2(%)
A	11.378	1.157	4	61.7
B	3.142	1.751	2.9	89.3
C	2.057	2.542	6.8	1.6
D	22.063	1.076	4.5	98.9
E	8.023	1.324	4.3	11.2
F	19.785	1.131	3.7	42.3
G	3.672	1.439	3.9	78.9
H	23.683	1.575	3.9	16.9
I	23.9	1.132	2.5	84.2

Fig. 8. Selected group of behavioral parameter sets and their calibration metrics that were used for model simulations. A nine behavioral parameter sets comprised of (*m* (m), *k*, *gw1* (%), and *gw2* (%)) were shown in table (upper right).

To address the equifinality concept, which states that there may be many models of a catchment that acceptably reproduce observations, we selected a group of behavioral parameter sets from the Monte Carlo simulations (Fig. 7) that had a percent error (*Qerr*) of $-5.0\% \leq Qerr \leq 5.0\%$, a Nash–Sutcliffe efficiency on daily flows ($NS \geq 0.75$), and a Nash–Sutcliffe efficiency on log daily flows ($NSlog \geq 0.60$). Nine behavioral parameter sets were identified that satisfied all the three mentioned conditions over the three different water year conditions (dry, average and wet). Fig. 8 gives a plot of the nine behavioral parameters sets selected with model performance metrics. In Fig. 8, we list at the upper right corner the nine behavioral parameters with values of *m* (m), *k*, *gw1* (%), and *gw2* (%). We give the model performance metrics corresponding to the different water years (dry, average, and wet) for
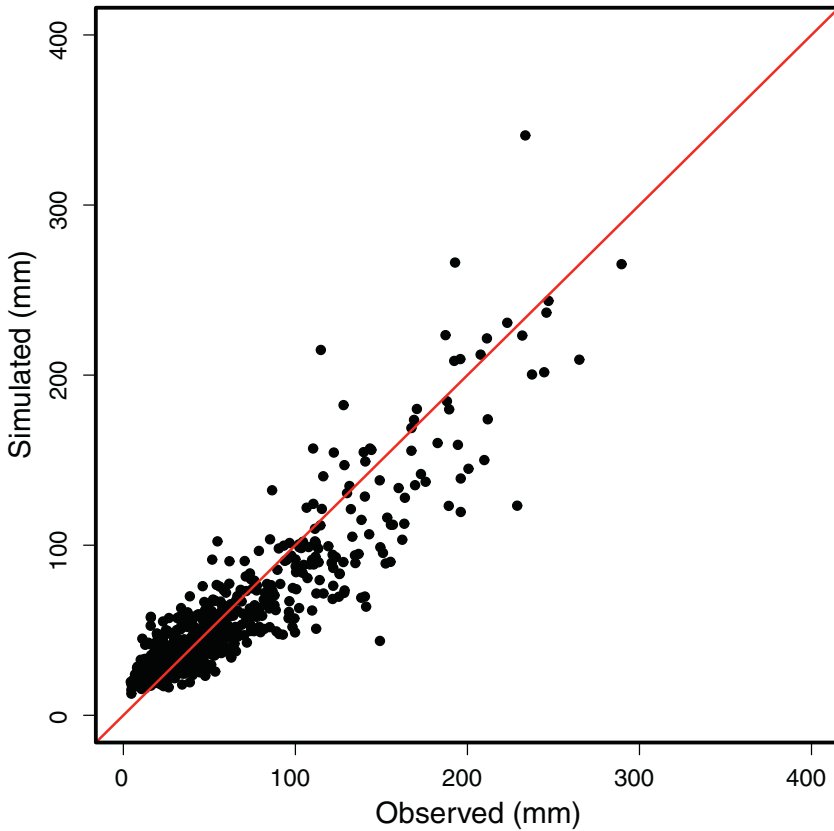
Fig. 9. Scatterplot of monthly observed and simulated runoff in mm for the Mad River near Moretown watershed (USGS gauge # 04288000) in verification of RHESSys during 1955 to 2010 water years. RHESSys parameters used to drive model simulations runoff results were: $m = 2.057$ (m), $k = 2.542$, $gw1 = 6.8$ (%), and $gw2 = 1.6$ (%).

each behavioral parameters set in red, green, and blue colors respectively. The model performance metrics shown in Fig. 8 are the Nash–Sutcliffe efficiency (NS) for daily simulated and observed runoff, the Nash–Sutcliffe efficiency ($NSlog$) for daily simulated and observed runoff in log-scale, and the percent error ($Qerr$) between daily simulated and observed runoff. We note that the average water year model solutions capture most of the variance observed compared with dry and wet years model solutions ($NS_{average} \approx 0.84$). Wet water year model solutions total annual flow error estimates achieved a close match with observed runoff values ($Qerr_{Wet} \approx 0\%$).

Fig. 9 shows monthly observed and simulated runoff for the study watershed as verification of RHESSys model performance during 1955–2010 water years. As seen in Fig. 9, model performance is robust. The verification period used was from water year 1955 to water year 2010. In general, all the selected behavioral parameter sets are able to explain more than 60% of the variance seen in observed daily runoff, and underestimate observed runoff by about 4%. Model results generated from each of the nine behavioral parameter sets show that patterns and trends of simulated runoff were consistent.

Simulated runoff results with $m = 23.9$ (m), $k = 1.132$, $gw1 = 2.5$ (%), and $gw2 = 84.2$ (%) parameter set (i.e., group I in Fig. 8) are able to explain about 79% of the variance seen in observed daily runoff during the calibration dry year, about 84% of the variance seen in observed daily runoff during the calibration average year, and about 79% of the variance seen in observed daily runoff during the calibration wet
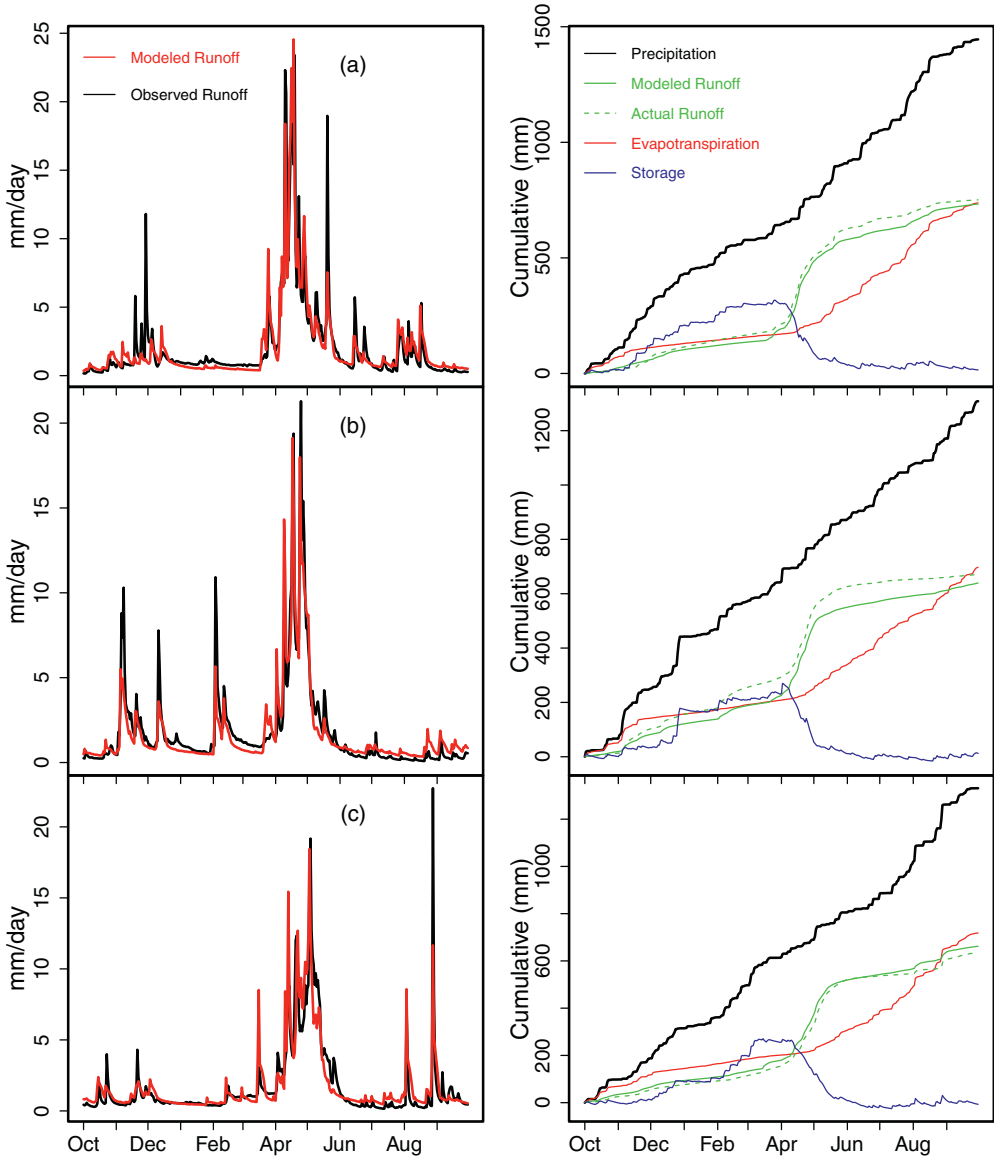
Fig. 10. Daily simulated versus observed runoff (mm) for the Mad River near Moretown watershed in calibration of RHESSys. Wet [row (a)], average [row (b)] and dry [row (c)] water yield year results are shown. Right panels give cumulative runoff (observed and simulated), evapotranspiration and storage simulated with observed precipitation during corresponding year to the left.

year (Fig. 10). Dry year water yield (panel a), average year water yield (panel b) and a wet year water yield (panel c) are shown in Fig. 10. We also present cumulative simulated runoff, evapotranspiration and storage (offset to be zero at the start) as well as observed precipitation and runoff. The model captures most of the variability seen in daily runoff during spring but to a lesser degree during summer time. This is shown with the Nash–Sutcliffe efficiency of log-transformed daily runoff values of 0.79 (panel a), 0.84 (panel b), and 0.76 (panel c).

Table 3

Annual precipitation at the Mad River watershed during 1951–2005 water years Mann Kendall trend analysis. μ is the arithmetic mean in meters, σ is unbiased standard deviation in meters, CV is coefficient of variation (σ/μ), ρ is correlation between gridded data (Maurer et al., 2002) and the CMIP5 ensemble, τ (tau) is Kendall's tau correlation coefficient, p-value is 2 sided-test, Trend is Highly Significant when ($p \leq 0.001$) and Significant when ($p \leq 0.05$).

| Data source/climate model ID	μ	σ	CV	ρ	τ (tau)	p-Value	Trend
Maurer et al.	1.209	0.192	0.159	–	0.3859	0.00003	Highly significant
ACCESS1-0	1.192	0.104	0.087	0.011	0.0128	0.89603	No trend
BCC-CSM1-1	1.189	0.108	0.091	0.077	0.0492	0.60119	No trend
BNU-ESM	1.199	0.113	0.095	0.318	0.2162	0.02018	Significant
CanESM2	1.193	0.117	0.098	0.064	0.0626	0.50421	No trend
CCSM4	1.200	0.105	0.088	−0.077	0.0303	0.74941	No trend
CESM1-BGC	1.200	0.094	0.079	0.208	0.2040	0.02835	Significant
CNRM-CM5	1.193	0.111	0.093	0.180	0.1960	0.03527	Significant
CSIRO-Mk3-6-0	1.203	0.133	0.111	0.126	−0.0020	0.98842	No trend
GFDL-CM3	1.200	0.101	0.084	−0.205	0.0626	0.50421	No trend
GFDL-ESM2G	1.197	0.099	0.082	0.025	0.1300	0.16337	No trend
GFDL-ESM2M	1.198	0.117	0.097	0.158	0.1582	0.08937	No trend
INM-CM4	1.189	0.107	0.090	−0.063	0.1205	0.19629	No trend
IPSL-CM5A-LR	1.201	0.111	0.092	0.168	0.2485	0.00755	Significant
IPSL-CM5A-MR	1.197	0.093	0.078	0.033	0.1098	0.23958	No trend
MIROC-ESM	1.194	0.093	0.078	−0.062	0.0909	0.33066	No trend
MIROC-ESM-CHEM	1.202	0.108	0.090	−0.161	0.0653	0.48586	No trend
MIROC5	1.184	0.123	0.104	0.008	−0.0397	0.67372	No trend
MPI-ESM-LR	1.196	0.112	0.094	0.075	0.0007	1.00000	No trend
MPI-ESM-MR	1.184	0.105	0.089	0.027	−0.0478	0.61134	No trend
MRI-CGCM3	1.198	0.100	0.083	0.124	0.1407	0.13105	No trend
NorESM1-M	1.195	0.082	0.068	0.079	0.2094	0.02442	Significant

3.2. Global climate models historical trends and variabilities

An analysis of twenty-one hindcast CMIP5 model output datasets was performed to assess the variability and trend of each dataset compared to the observed historical data of Maurer et al. (2002). The precipitation coefficient of variation (CV) and trend (represented by Kendall's tau) are presented in Table 3. As noted by the discrepancy in Kendall's tau compared to the observations, none of the CMIP5 datasets adequately reproduces the observed precipitation trend. Only five CMIP5 model outputs show a statistically significant increasing trend (which is far lower in magnitude than the observed), and those five are chosen as a subset on that basis for further analysis in this work. Moreover, comparison of the precipitation coefficient of variation of the CMIP5 and observed data sets shows that none of the CMIP5 models adequately reproduces the observed variability, which limits the ability to simulate extreme events.

The failure of the hindcast climate data to reproduce the observed trend calls into question the validity of the precipitation forecast data as an adequate driver of hydrology models for the simulation of climate change impacts. Therefore, for an alternate scenario, we superimposed the observed trend in the historical precipitation (+7 mm/year) on the relatively flat CMIP5 precipitation data for use as a driver of the hydrology model presented in this work. This approach assumes that the observed trend will continue unchanged in the future, and allows assessment of the possible hydrologic flow regime resulting from increasing precipitation. Hydrology model simulation results using both altered and unaltered precipitation input time series are compared to emphasize the importance of trend in the CMIP5 data. The CMIP5 products reproduce observed temperature trends, which were left unaltered.

The RHESSys model was run in a retrospective mode to produce historical runoff simulations using the historical CMIP5 climate data (1955–2005) as a climate driver. The annual runoff simulations (retrospective climate data from five climate models under two scenarios) show a different trend and variability when compared to historical observed runoff data (Fig. 11). Fig. 11 shows both time series as well as distributions (represented by boxplots) to illustrate these differences in trend and variability. Mean annual runoff from all climate models was close to observed runoff. However, interquartile annual runoff range of all climate models tested was less than observed annual runoff. Not surprisingly,
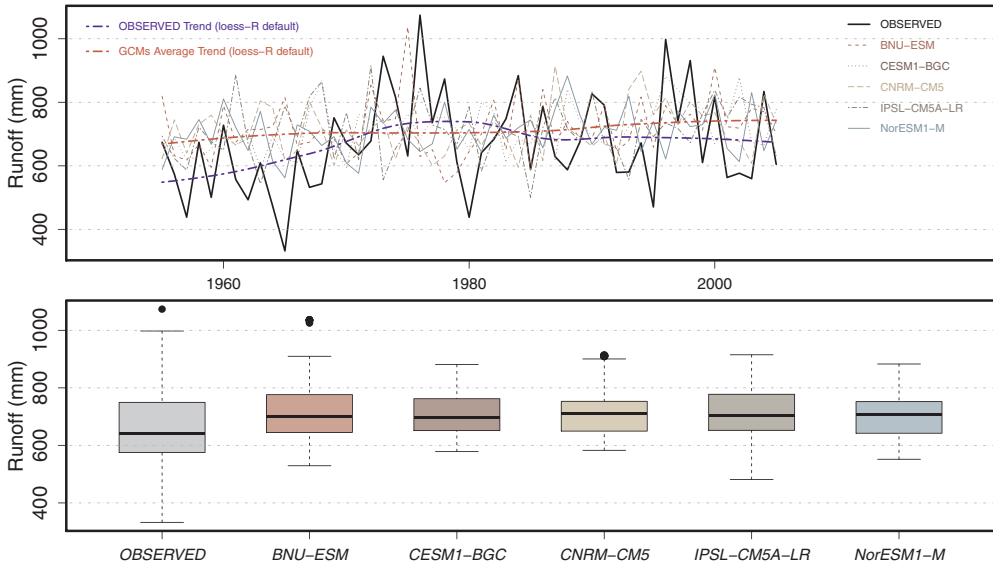
Fig. 11. Annual observed and retrospective simulated runoff at the Mad River near Moretown watershed (USGS gauge # 04288000). Data are runoff for the water years 1955–2005. Runoff simulations were obtained by hindcasting the RHESSys model with five climate models from the CMIP5 ensembles data and the nine behavioral sets discussed. Trends shown were obtained using the local polynomial regression fitting (loess) function with default parameters in *R* software package.

climate model-driven runoff simulations have clearly underestimated the historical observed runoff trend because of the lack of trend in CMIP5 precipitation data. Differences in trends are visualized using local polynomial regression fitting function (loess) evaluated from the default parameters in the *R* software package (Cleveland et al., 1992; R Development Core Team, 2014). These results (Fig. 11) show that climate model data have not succeeded in producing historical observed runoff trends and variabilities when applied on a regional scale study.

3.3. Model prediction

Runoff simulations shown in Figs. 12–15 were obtained by driving the RHESSys model with ensembles from: (i) the subset of five CMIP5 climate models that show significant trend in precipitation, and (ii) the five climate models from the CMIP5 with the superimposed trend as described earlier (Section 2.3). In both of the two sets of ensembles, we considered the two climate scenarios (*RCP 4.5* and *RCP 8.5*). The five climate models shown in Figs. 12–15 are, a: *BNU—ESM*; b: *CESM1—BGC*; c: *CNRM—CM5*; d: *IPSL—CM5A—LR*; and e: *NorESM1—M*. A noticeable increase in number of flooded days has been observed. In addition, a repeated pattern of flood occurrences is evident across all the climate model studies with variations in duration.

Fig. 12 shows kernel density estimates of the distribution of maximum flood duration days at our study watershed, using the flood threshold of 15 mm/day (2,175 cfs). The 1964–2013 line in Fig. 12 is the kernel density estimate of flood duration days using the flood threshold of 15 mm/day during 1964–2013 water years. Future (i.e., 2016–2099 water years) kernel density estimates of flood duration days were obtained by driving the RHESSys model with five climate models from the CMIP5 ensembles (subscript 1) as well as the superimposed trend ensembles (subscript 2) considering the two scenarios (i.e., *RCP 4.5* and *RCP 8.5*) and the nine behavioral sets discussed. The estimated bandwidth that the Sheather and Jones (1991) method gives for the various distributions shown in Fig. 12 vary between 0.1 and 1.7 days. For consistency, so that mode differences are not due to bandwidth differences, Fig. 12 was plotted using the average bandwidth of 0.8 days. To check sensitivity to bandwidth, we also plotted density estimates with range of bandwidths spanning 0.1–1.7 days and obtained figures (not shown)
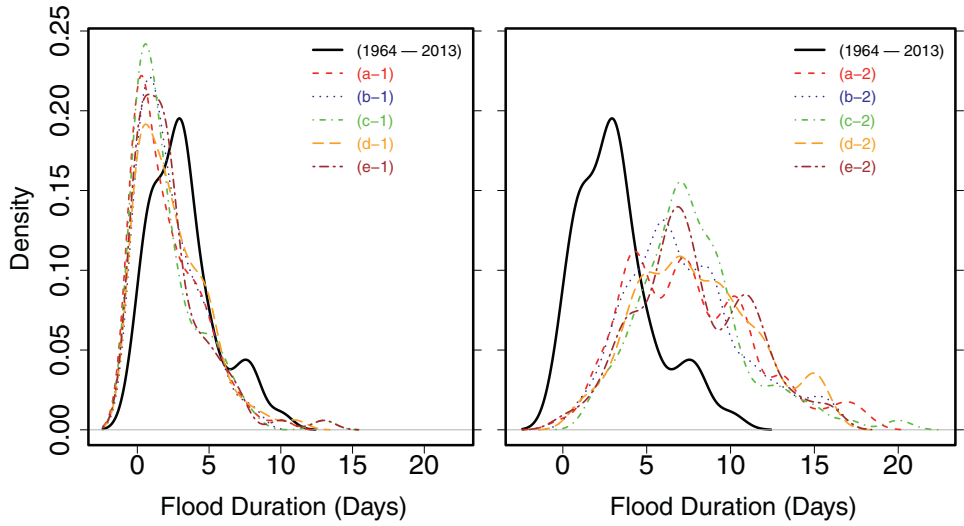
Fig. 12. Kernel density estimate of the flood duration in days at the Mad River near Moretown watershed (USGS gauge # 04288000) observed and projected from model simulations. The flood duration in days are the number of days when runoff equals or exceeds a runoff magnitude of 15 mm/day (i.e., daily discharge of 2,175 cfs). Kernel density line labeled (b-1) refers to the *CESM1−BGC* climate model ensembles flood duration scenario, while kernel density line labeled (c-2) refers to the *CNRM−CM5* climate model with superimposed trend ensembles flood duration scenario.
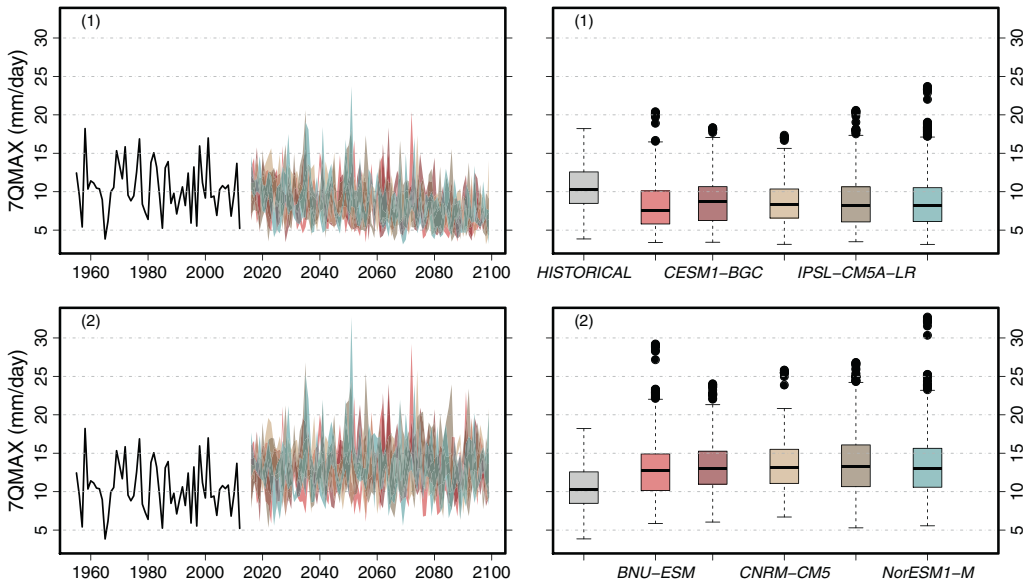

Fig. 13. Seven-day maximum flow at the Mad River near Moretown watershed (USGS gauge # 04288000). Right panels give boxplots of seven-day maximum (*7QMAX*) data for the historical (1955–2013) and simulated (2016–2099) water year runoffs. Panels numbered with 1 refer to the CMIP5 ensembles, while panels numbered with 2 refer to the CMIP5 with superimposed trend ensembles.
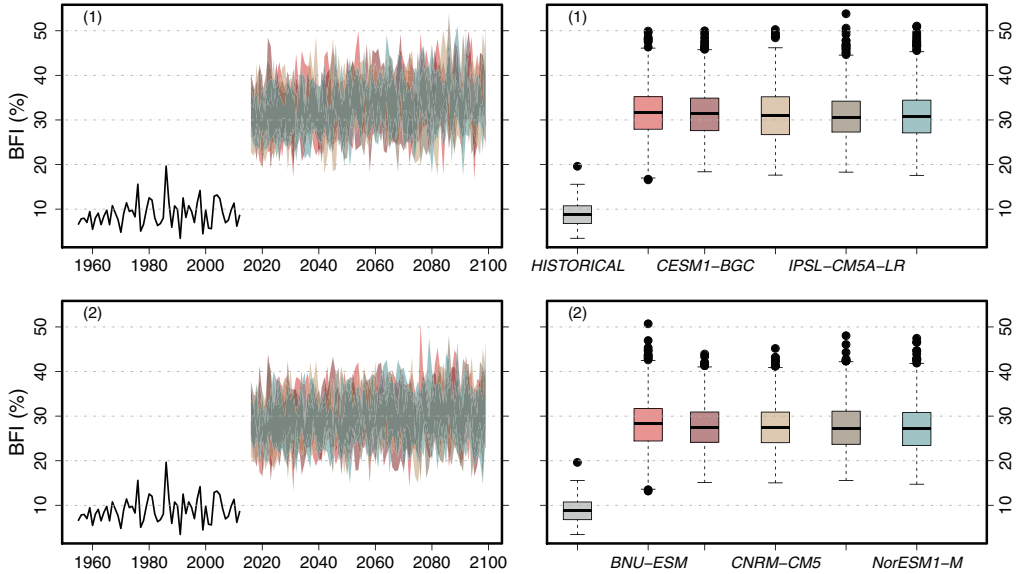
Fig. 14. Base flow index (*BFI*) at the Mad River near Moretown watershed (USGS gauge # 04288000). Right panels give boxplots of base flow index data for the historical (1955–2013) and simulated (2016–2099) water year runoffs. Panel number follows naming convention used earlier in Fig. 13.

that were very similar to Fig. 12, with modes at the same locations. We therefore concluded that interpretations were not sensitive to the selection of bandwidth in the range resulting from different data lengths. We also looked at time series plots for the abovementioned distributions (not shown) and found that roughly every 25 years there is a peak in number of flooded days. Our results, using
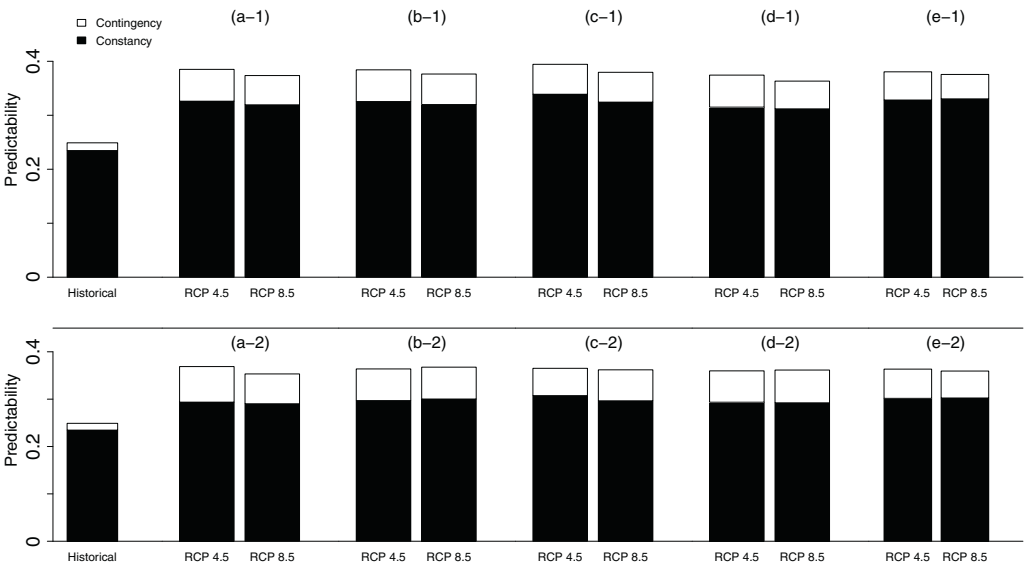
Fig. 15. Colwell index, Predictability (*P*), Constancy (*C*), and Contingency (*M*) of runoff at the Mad River near Moretown watershed (USGS gauge # 04288000). Data are daily runoff for the water years 1955–2013 (historical) and simulated runoff for the water years 2016–2099 (future). Panel number follows naming convention used earlier in Fig. 12.

a superimposed increasing precipitation trend reflected in the historical record, predict four more flooded days in the coming century relative to the hindcast period.

Using the unaltered CMIP5 data as input (*RCP 4.5* and *RCP 8.5*), model results do not show a significant change in the highest flows (*7QMAX*), despite future projections of increased precipitation in the region (Fig. 13, part 1). This may represent the role of soil moisture or snowpack dynamics. However, a significant change is shown for the case of superimposed precipitation trend ensembles. Results suggest that the median of the seven maximum runoff *7QMAX* will change by 30% in the future (Fig. 13, part 2).

We also assessed climate-induced changes in low flow disturbances. Our results suggest that both variables that quantify low flow disturbances (*BFI* and *7QMIN*) showed a significant increase in the future. We noted an increase of about three orders of magnitude in the base flow index variable (Fig. 14). This increase in low flow regime is evident through the use of all the climate models studied. In Fig. 14, we show boxplots of historic and future base flow indices to illustrate the degree of increased change. The timing associated with this increase is during summer (June 21th to September 20th). The 7-day minimum (*7QMIN*) variable behavior has not been shown since it conveys the same information. This finding is consistent with the recent observation of Hodgkins and Dudley (2011) indicating that the latter half of the twentieth century has witnessed an increase in summer flows in New England.

Model predictions did not indicate a significant change in flow reversal days under future climate scenarios. Some models suggest decreased number of reversal days while others suggest increased number of reversal days. We think that the quality of our prediction results did not succeed to manifest a clear flow variability signal (input climate data and model efficiency to capture streamflow variance). These results convey a limitation of our modeling efforts to assess stream banks damages anticipated with climate change.

Model output shows a 60% increase in the Colwell index runoff predictability metric for the 2015–2099 water years period among all models tested. Both constancy and contingency are shown as bar plots in Fig. 15 to illustrate the Colwell index components. We note that the contingency is minimal which means that the probability of occurrence of each flow state is independent of the month (homogenous monthly flow time series). We infer that expected runoff at this study watershed would have a different monthly pattern or distribution compared to historical data observed. Monthly runoff pattern change will affect the quality of the watershed habitat and cause ecological consequences on fisheries populations.

4. Discussion

The CMIP5 data products (Taylor et al., 2011; Meehl et al., 2014) are widely used for regional climate change impacts analysis. However, for our study area in northwestern New England, only five climate models showed statistically significant trends in precipitation in hindcast, but the magnitude of these trends are not adequately representative of those seen in observed annual precipitation. To address this discrepancy in historical precipitation trend, we extrapolated the observed historical precipitation trend to provide an upper envelope of predictions of future hydrological impacts associated with climate change. The use of an extrapolated observed trend cannot capture regional climate patterns induced by large-scale changes in circulation or decadal-scale climatic oscillations (such as the North Atlantic Oscillation or Arctic Oscillation), and therefore future datasets with extrapolated trends must be used with great caution. However, it is clear from this analysis that CMIP5 products are insufficient for regional hydrologic analysis in Vermont because the trend and variability are underrepresented. The use of any of the twenty-one CMIP5 models available would lead to runoff simulations that show no change in high flows. Such a conclusion could erroneously be used as a basis for a "do nothing" approach by policy makers for adaptation to climate change, when in fact increasing precipitation can cause numerous adverse hydrologic impacts, such as an increased flood risk and exacerbated nonpoint source pollution. We demonstrate the large difference in flow regime when using the CMIP5 data with a superimposed trend compared to only unaltered CMIP5 data using the best five datasets. The near-term (4–5 decades) predicted flows using the superimposed trend dataset may be useful for design and planning as a basic scenario for adaptation to climate change in high gradient watersheds in northwestern New England.

In addition to the lack of a reproduced trend in precipitation, recent work has described the failure of the CMIP5 data to capture increased intensity, duration and frequency of precipitation extremes, which is consistent with our finding of inadequate representation of variability in the precipitation process in Vermont (Wuebbles et al., 2013). Therefore, the changing probability of the uppermost quantiles is not well represented using our approach. The mean, variability, and skewness of flow are all expected to change with climate change, but the presented approach only allows for changes in the first two moments.

Our approach to projecting future flow regime in northwestern New England has not incorporated the nonlinear interconnectivity and feedbacks between climate variables and vegetation cover. Moreover, the hydrological model used in our approach did not include incorporation of impacts of increased CO_2 concentrations on stomatal physiology of forests, changes in species composition or distribution, and the response of leaf area index to climate change. Vegetation feedbacks could act in various ways to exacerbate or offset our projected changes in streamflow. CO_2 fertilization would be expected to reduce stomatal conductance and increase water use efficiency, thereby decreasing evapotranspiration (ET) and increasing streamflow during the growing season, as discussed by Campbell et al. (2011), though their model projections of streamflow incorporating CO_2 fertilization resulted in increasing trends in future ET at the Hubbard Brook Experimental Forest in nearby New Hampshire. Warmer conditions in the future might alternatively lengthen the growing season for forests in the region (Betts, 2011; Richardson et al., 2012; White et al., 2014). A future trend of lengthened leaf-on period would result in days to weeks of extended ET, offsetting some of the increased future precipitation and mitigating against increasing baseflow. A more complex and yet unexamined impact of climate change on vegetation-water relations would be associated with changes in forest health and species composition that would drive changes in ET demands and resulting streamflow. Declining forest health and associated reductions in ET could lead to increases in baseflow greater than the levels we project here. The step changes in the base flow index projected in our simulations are driven by the projected linear trend in increasing precipitation and do not include these more complex vegetation-climate interactions that may alter future streamflows. In general, our ability to project flow regime should be assessed considering this uncertainty.

Our results suggest a repeated pattern of flood occurrences with increased frequency. Some studies have suggested that this repeated mode of flood occurrences in our study region is correlated with climate index occurrences at the region such as the North Atlantic Oscillation (NAO) (Huntington et al., 2004; Griffiths and Bradley, 2007; Brown et al., 2010). This repeated phenomenon of flood occurrences may likely be attributed to hemispheric scale and potentially regional scale atmospheric circulation patterns, however the expected warmed climate may influence these atmospheric circulation indices themselves, hence there is great uncertainty in future flood signals (Visbeck et al., 2001).

Flow variability is an important aspect of the streamflow regime. There is an ongoing discussion within the Lake Champlain management community as well as the state and federal environmental protection agencies concerning the Lake Champlain sediment and nutrient loads (Stager and Thill, 2010). The anticipated future increased maximum flows will likely greatly exceed current sediment and nutrient loading to the Lake, continuing a trend of declining water quality in Lake Champlain (Lake Champlain Basin Program, 2012).

The Mad River watershed physical habitat is for Brown and Brook trout, Longnose dace, and Slimy sculpin but in some reaches, the water quality limits fish populations. Fish populations inhabiting Vermont streams and rivers in general have adapted to flooding (Kirn, 2011). However, given the expected changes in climate (temperature increase) and the associated streamflow temporal patterns change (Colwell's predictability increase) the future adaptation should be considered. The anticipated hydrological impacts presented herein may assist ongoing research that investigates these ecological responses to climate change in Lake Champlain ecosystem (Warren et al., 2012).

The presented work critically assesses the ability of the CMIP5 ensemble to adequately capture the dynamics of climate conditions over the historic period at our study region for use in hydrologic impact analysis. Our future simulation results highlight the substantial differences between the use of CMIP5 and trend-extrapolated observations, underscoring the need to be very cautious when applying climate model products for regional analysis. However, the prediction results presented in this work should be viewed as best estimates of what is available. Understanding changes in streamflow regime

requires a better knowledge of climate data, runoff models parameters, and representation of physical processes. In order to obtain that knowledge, extensive field efforts intended to examine hydrological model sensitivities to climate and hydrological model parameters are required.

5. Conclusions

Using the CMIP5 climate data for regional hydrologic analysis to make runoff projections to inform planning and policy would be fundamentally problematic if the climate models are not adequately validated for a region of interest. Many of the forcing CMIP5 data fail to capture both the trends and variability observed in precipitation when run in hindcast. This study has shown the potential differences in simulated flow metrics if the CMIP5 data is applied uncritically, and shows that CMIP5 fails to capture trends toward increased precipitation in Vermont.

Nevertheless, when driven by the CMIP5 data corrected for trend, the hydrological model used in this study predicts an increase in high flows, low flows, and a decrease in the uncertainty seen in temporal patterns of runoff during the 21st century for central Vermont. The trend-corrected simulation shows an increase of 30% in seven-day maximum flow, four days increase in flooded days, three orders of magnitude increase in base flow index, and a 60% increase in runoff predictability. The above-mentioned results reflect the need to adapt to increased flood risk, updated floodplain management, exacerbated nonpoint pollution loading to Lake Champlain, and other problems associated with higher future flows.

Acknowledgements

Appendix A.

The World Climate Research Programme (WCRP) developed global climate projections through its Coupled Model Intercomparison Project 5 (CMIP5). We examined twenty-one projection ensembles of CMIP5 downscaled by the daily bias-correction and constructed analogs (*BCCA*) statistical downscaling technique available at (http://gdo-dcp.ucllnl.org/downscaled_cmip_projections/) accessed on 27 May 2014 and listed in Table A1. Mann Kendall trend analysis (Helsel and Hirsch, 2002) was used to examine whether any trends in precipitation data were statistically significant. Table 3 gives trend analysis results for the historic observed annual precipitation (Maurer et al., 2002) as well as the CMIP5 projection ensembles hindcast data over our study watershed. This table includes the mean annual precipitation, μ, the annual standard deviation, σ, the coefficient of variation, *CV*, the cross correlation between climate model ensembles and observed precipitation, ρ, the Kendall's tau correlation coefficient, τ, as well as the *p-value* associated with the Mann Kendall test. Table 3 shows that they are five climate model ensembles with significant increasing trend ($p < 0.05$) in annual precipitation. Namely, these five climate modeling centers are: the College of Global Change and Earth System Science, Beijing Normal University (*BNU—ESM*); the Community Earth System Model Contributors (*CESM1—BGC*); the Centre National de RecherchesMétéorologiques/Centre Européen de Recherche et Formation Avancée en CalculScientifique (*CNRM—CM5*); the Institut Pierre-Simon Laplace (*IPSL—CM5A—LR*); and the Norwegian Climate Centre (*NorESM1—M*). Among the twenty-one projection ensembles analyzed, these

Table A1
Coupled Model Intercomparison Project (CMIP5) groups studied.

No.	Modeling center (or group)	Institute ID	Model name
1	Commonwealth Scientific and Industrial Research Organization and Bureau of Meteorology, Australia	CSIRO-BOM	ACCESS1-0
2	Beijing Climate Center, China Meteorological Administration	BCC	BCC-CSM1-1
3	College of Global Change and Earth System Science, Beijing Normal University	GCESS	BNU-ESM
4	Canadian Centre for Climate Modelling and Analysis	CCCMA	CanESM2
5	National Center for Atmospheric Research	NCAR	CCSM4
6	Community Earth System Model Contributors	NSF-DOE-NCAR	CESM1-BGC
7	Centre National de Recherches Météorologiques/Centre Européen de Recherche et Formation Avancée en Calcul Scientifique	CNRM-CERFACES	CNRM-CM5
8	Commonwealth Scientific and Industrial Research Organization, Queensland Climate Change Centre of Excellence	CSIRO-QCCCE	CSIRO-Mk3.6.0
9	NOAA Geophysical	NOAA GDFL	GFDL-CM3
10	Fluid Dynamics		GFDL-ESM2G
11	Laboratory		GFDL-ESM2M
12	Institute for Numerical Mathematics	INM	INM-CM4
13	Institut Pierre-Simon	IPSL	IPSL-CM5A-LR
14	Laplace		IPSL-CM5A-MR
15	Japan Agency for Marine-Earth Science and	MIROC	MIROC-ESM
16	Technology, Atmosphere and Ocean Research Institute (The University of Tokyo), and National Institute for Environmental Studies		MIROC-ESM-CHEM
17	Atmosphere and Ocean Research Institute (The University of Tokyo), National Institute for Environmental Studies, and Japan Agency for Marine-Earth Science and Technology	MIROC	MIROC5
18	Max-Planck-Institut für Meteorologie (Max	MPI-M	MPI-ESM-LR
19	Planck Institute for Meteorology)		MPI-ESM-MR
20	Meteorological Research Institute	MRI	MRI-CGCM3
21	Norwegian Climate Centre	NCC	NorESM1-M

five models showed a relatively close correlation with observed precipitation data. We adopted using these five climate model ensembles for this work.

Appendix B.

Flow predictability variables used in this paper are *Colwell's* indices (Colwell, 1974). *Colwell's* indices are predictability (*P*), constancy (*C*) and contingency (*M*). Constancy (*C*) and contingency (*M*) are quantified based on entropy measures of uncertainty from Shannon's information theory either across all months (*C*), or contingent upon a specific month (*M*) (Jelínek, 1968). Predictability (*P*) has two separable components: constancy (*C*) and contingency (*M*). Predictability combines constancy and contingency through $P = C + M$. Calculation of *Colwell's* indices *P*, *C* and *M* requires that values be binned into discrete groups.

Predictability (*P*) is the converse of uncertainty, it is reasonable then to base measures of predictability and its components, constancy (*C*) and contingency (*M*), on the mathematics of information theory (Colwell, 1974). Following *Colwell*, for a frequency matrix (contingency table) with *t* columns (times within a cycle) and *s* rows (state of the phenomenon). Let N_{ij} be the number of cycles for which the

phenomenon was in state i at time j. Define the column totals (X_j), row totals (Y_i), and the grand total (Z) as:

$$X_j = \sum_{i=1}^{s} N_{ij},$$

$$Y_i = \sum_{j=1}^{t} N_{ij},$$

and $Z = \sum_i \sum_j N_{ij} = \sum_j X_j = \sum_i Y_i.$

Then the uncertainty with respect to time is

$$H(X) = -\sum_{j=1}^{t} \frac{X_j}{Z} \log \frac{X_j}{Z},$$

the uncertainty with respect to state is

$$H(Y) = -\sum_{i=1}^{s} \frac{Y_i}{Z} \log \frac{Y_i}{Z},$$

and the uncertainty with respect to the interaction of time and state is

$$H(XY) = -\sum_i \sum_j \frac{N_{ij}}{Z} \log \frac{N_{ij}}{Z}.$$

The predictability of a periodic phenomenon is maximal when there is complete certainty with regard to state (row) once the point in time (column) is specified. In terms of information theory, the conditional uncertainty with regard to state, with time given, is defined as (Jelínek, 1968)

$$H_X(Y) = H(XY) - H(X).$$

When predictability is at its minimum, all states are equiprobable for all times. In this case $H(X) = \log t$, and $H(XY) = \log st$, so that $H_X(Y) = \log s$. To obtain measure of predictability (P) with the range (0,1), define

$$P = 1 - \frac{H_X(Y)}{\log s} = 1 - \frac{H(XY) - H(X)}{\log s}.$$

Constancy is maximized when all row totals but one are zero; it is minimized when all row totals are equal. Since $H(Y)$ varies in precisely the opposite way, and its maximum value is $\log s$, a measure of constancy (C) with range (0,1) is given by

$$C = 1 - \frac{H(Y)}{\log s}.$$

Contingency represents the degree to which time determines state, or the degree to which they are dependent on each other. In information theory, contingency is measured by a quantity called average mutual information (Jelínek, 1968). Colwell (1974) cites contingency as the average amount of information about the state of the phenomenon provided by time or $I(XY) = H(Y) - H_X(Y) = H(Y) + H(X) - H(XY).$

Colwell (1974) gives an adjusted measure of contingency (M), with range (0,1) as

$$M = \frac{H(X) + H(Y) - H(XY)}{\log s}.$$

References

Band, L.E., Patterson, P., Nemani, R., Running, S.W., 1993. Forest ecosystem processes at the watershed scale: incorporating hillslope hydrology. Agric. Forest Meteorol. 63, 93–126, http://dx.doi.org/10.1016/0168-1923(93)90024-C.

Band, L.E., Mackay, D.S., Creed, I.F., Semkin, R., Jeffries, D., 1996. Ecosystem processes at the watershed scale: sensitivity to potential climate change. Limnol. Oceanogr. 41, 928–938, http://dx.doi.org/10.4319/lo.1996.41.5.0928.

Betts, A.K., 2011. Vermont climate change indicators. Weather Climate Soc. 3, 106–115, http://dx.doi.org/10.1175/2011WCAS1096.1.

Brekke, L., Thrasher, B.L., Maurer, E., Pruitt, T., 2013. Downscaled CMIP3 and CMIP5 Climate Projections: Release of Downscaled CMIP5 Climate Projections, Comparison with Preceding Information, and Summary of User Needs. U.S. Dept. of the Interior Tech. Rep., BOR, Denver.

Brown, P.J., Bradley, R.S., Keimig, F.T., 2010. Changes in extreme climate indices for the northeastern United States, 1870–2005. J. Climate 23, 6555–6572, http://dx.doi.org/10.1175/2010jcli3363.1.

Campbell, J.L., Driscoll, C.T., Pourmokhtarian, A., Hayhoe, K., 2011. Streamflow responses to past and projected future changes in climate at the Hubbard Brook Experimental Forest, New Hampshire, United States. Water Resour. Res. 47, W02514, http://dx.doi.org/10.1029/2010wr009438.

Chinnayakanahalli, K.J., Hawkins, C.P., Tarboton, D.G., Hill, R.A., 2011. Natural flow regime, temperature and the composition and richness of invertebrate assemblages in streams of the western United States. Freshwater Biol. 56, 1248–1265, http://dx.doi.org/10.1111/j.1365-2427.2010.02560.x.

Cleveland, W.S., Grosse, E., Shyu, W.M., 1992. Local regression models. In: Chambers, J.M., Hastie, T.J. (Eds.), Statistical Models in S. Wadsworth & Brooks/Cole, Pacific Grove, CA, p. 608.

Colwell, R.K., 1974. Predictability, constancy, and contingency of periodic phenomena. Ecology 55, 1148–1153, http://dx.doi.org/10.2307/1940366.

Dingman, S.L., 2002. Physical Hydrology, 2nd ed. Prentice Hall, Upper Saddle River, NJ, 646 pp.

Dunne, T., Leopold, L.B., 1978. Water in Environmental Planning. W.H. Freeman and Company, New York, 818 pp.

Gibson, C.A., Meyer, J.L., Poff, N.L., Hay, L.E., Georgakakos, A., 2005. Flow regime alterations under changing climate in two river basins: implications for freshwater ecosystems. River Res. Appl. 21, 849–864, http://dx.doi.org/10.1002/rra.855.

Gordon, N.D., McMahon, T.A., Finlayson, B.L., Gippel, C.J., Nathan, R.J., 2004. Stream Hydrology: An Introduction for Ecologists, 2nd ed. John Wiley & Sons, Chichester, England, 429 pp.

GRASS Development Core Team, 2012. Geographic Resources Analysis Support System (GRASS) Software, Version 6.4.2. Fondazione Mach – Centre for Alpine Ecology CEA, Trento, Italy, Available at: http://grass.osgeo.org/

Griffiths, M.L., Bradley, R.S., 2007. Variations of twentieth-century temperature and precipitation extreme indicators in the northeast United States. J. Climate 20, 5401–5417, http://dx.doi.org/10.1175/2007jcli1594.1.

Hartley, S., Dingman, S.L., 1993. Effects of climatic variability on winter-spring runoff in New England river basins. Phys. Geogr. 14, 379–393.

Hauer, F.R., Baron, J.S., Campbell, D.H., Fausch, K.D., Hostetler, S.W., Leavesley, G.H., Leavitt, P.R., McKnight, D.M., Stanford, J.A., 1997. Assessment of climate change and freshwater ecosystems of the Rocky Mountains, USA and Canada. Hydrol. Process. 11, 903–924, http://dx.doi.org/10.1002/(sici)1099-1085(19970630)11:8<903::aid-hyp511>3.0.co;2-7.

Hayhoe, K., Wake, C., Huntington, T., Luo, L., Schwartz, M., Sheffield, J., Wood, E., Anderson, B., Bradbury, J., DeGaetano, A., Troy, T., Wolfe, D., 2007. Past and future changes in climate and hydrological indicators in the US northeast. Clim. Dynam. 28, 381–407, http://dx.doi.org/10.1007/s00382-006-0187-8.

Hayhoe, K., Wake, C., Anderson, B., Liang, X.-Z., Maurer, E., Zhu, J., Bradbury, J., DeGaetano, A., Stoner, A., Wuebbles, D., 2008. Regional climate change projections for the Northeast USA. Mitig. Adapt. Strat. Global Change 13, 425–436, http://dx.doi.org/10.1007/s11027-007-9133-2.

Helsel, D.R., Hirsch, R.M., 2002. Statistical Methods in Water Resources Techniques of Water Resources Investigations, Book 4. U.S. Geol. Sur., Reston, VA (Chapter A3), 510 pp.

Hodgkins, G.A., Dudley, R.W., Huntington, T.G., 2003. Changes in the timing of high river flows in New England over the 20th Century. J. Hydrol. 278, 244–252, http://dx.doi.org/10.1016/s0022-1694(03)00155-0.

Hodgkins, G.A., Dudley, R.W., 2005. Changes in the magnitude of annual and monthly streamflows in New England, 1902–2002. U.S. Geol. Surv. Sci. Invest. Rep., 2005–5135.

Hodgkins, G.A., Dudley, R.W., Huntington, T.G., 2005. Summer low flows in New England during the 20th century. J. Am. Water Resour. Assoc. 41, 403–411, http://dx.doi.org/10.1111/j.1752-1688.2005.tb03744.x.

Hodgkins, G.A., Dudley, R.W., 2006. Changes in the timing of winter-spring streamflows in eastern North America, 1913–2002. Geophys. Res. Lett. 33, L06402, http://dx.doi.org/10.1029/2005GL025593.

Hodgkins, G.A., Dudley, R.W., 2011. Historical summer base flow and stormflow trends for New England rivers. Water Resour. Res. 47, W07528, http://dx.doi.org/10.1029/2010WR009109.

Huntington, T.G., Hodgkins, G.A., Keim, B.D., Dudley, R.W., 2004. Changes in the proportion of precipitation occurring as snow in New England (1949–2000). J. Climate 17, 2626–2636, http://dx.doi.org/10.1175/1520-0442(2004)017<2626:CITPOP>2.0.CO;2.

Huntington, T.G., Richardson, A.D., McGuire, K.J., Hayhoe, K., 2009. Climate and hydrological changes in the northeastern United States: recent trends and implications for forested and aquatic ecosystems. Can. J. Forest Res. 39, 199–212, http://dx.doi.org/10.1139/x08-116.

Jelínek, F., 1968. Probabilistic Information Theory: Discrete and Memoryless Models. McGraw-Hill, New York, 609 pp.

Kaufmann, M.R., Troendle, C.A., 1981. The relationship of leaf area and foliage biomass to sapwood conducting area in four subalpine forest tree species. Forest Sci. 27, 477–482.

Kirn, R., 2011. Flood Impacts to Wild Trout Populations in Vermont. Vermont Agency of Natural Resources Fisheries Programs Rep., VDFW, Roxbury, VT.

Lake Champlain Basin Program, 2012. State of the Lake and Ecosystems Indicators. LCBP Annual Rep., Grand Isle, VT.

Lazzaro, G., Basso, S., Schirmer, M., Botter, G., 2013. Water management strategies for run-of-river power plants: profitability and hydrologic impact between the intake and the outflow. Water Resour. Res. 49, 8285–8298, http://dx.doi.org/10.1002/2013wr014210.

Maurer, E.P., Wood, A.W., Adam, J.C., Lettenmaier, D.P., Nijssen, B., 2002. A long-term hydrologically based dataset of land surface fluxes and states for the conterminous United States. J. Climate 15, 3237–3251, http://dx.doi.org/10.1175/1520-0442(2002)015<3237:ALTHBD>2.0.CO;2.

Maurer, E.P., Hidalgo, H.G., Das, T., Dettinger, M.D., Cayan, D.R., 2010. The utility of daily large-scale climate data in the assessment of climate change impacts on daily streamflow in California. Hydrol. Earth Syst. Sci. 14, 1125–1138, http://dx.doi.org/10.5194/hess-14-1125-2010.

Meehl, G.A., Covey, C., Taylor, K.E., Delworth, T., Stouffer, R.J., Latif, M., McAvaney, B., Mitchell, J.F.B., 2007. The WCRP CMIP3 Multimodel dataset: a new era in climate change research. Bull. Am. Meteorol. Soc. 88, 1383–1394, http://dx.doi.org/10.1175/BAMS-88-9-1383.

Meehl, G.A., Moss, R., Taylor, K.E., Eyring, V., Stouffer, R.J., Bony, S., Stevens, B., 2014. Climate model intercomparisons: preparing for the next phase. EOS Trans. AGU 95, 77–78, http://dx.doi.org/10.1002/2014EO090001.

Melack, J.M., Dozier, J., Goldman, C.R., Greenland, D., Milner, A.M., Naiman, R.J., 1997. Effects of climate change on inland waters of the Pacific coastal mountains and western Great Basin of north America. Hydrol. Process. 11, 971–992, http://dx.doi.org/10.1002/(SICI)1099-1085(19970630)11:8<971::AID-HYP514>3.0.CO;2-Y.

Melillo, J.M., Richmond, T.T.C., Yohe, G.W., 2014. Climate Change Impacts in the United States, U.S. National Climate Assessment 3rd Rep. U.S. Global Change Res. Prog., Washington, DC, http://dx.doi.org/10.7930/J0Z31WJ2.

Moore, M.V., Pace, M.L., Mather, J.R., Murdoch, P.S., Howarth, R.W., Folt, C.L., Chen, C.Y., Hemond, H.F., Flebbe, P.A., Driscoll, C.T., 1997. Potential effects of climate change on freshwater ecosystems of the New England/Mid-Atlantic region. Hydrol. Process. 11, 925–947, http://dx.doi.org/10.1002/(SICI)1099-1085(19970630)11:8<925::AID-HYP512>3.0.CO;2-X.

Mulholland, P.J., Best, G.R., Coutant, C.C., Hornberger, G.M., Meyer, J.L., Robinson, P.J., Stenberg, J.R., Turner, R.E., Vera-Herrera, F., Wetzel, R.G., 1997. Effects of climate change on freshwater ecosystems of the south-eastern United States and the Gulf coast of Mexico. Hydrol. Process. 11, 949–970, http://dx.doi.org/10.1002/(SICI)1099-1085(19970630)11:8<949::AID-HYP513>3.0.CO;2-G.

Myers, C.A., Edminster, C.B., 1972. Volume tables and point-sampling factors for Engelmann spruce in Colorado and Wyoming. In: U.S. Forest Service RP-Rep. 95. Rocky Mtn. Forst. & Range Exp. Stat.

Poff, N., 1996. A hydrogeography of unregulated streams in the United States and an examination of scale-dependence in some hydrological descriptors. Freshwater Biol. 36, 71–79, http://dx.doi.org/10.1046/j.1365-2427.1996.00073.x.

Poff, N.L., Ward, J.V., 1989. Implications of streamflow variability and predictability for lotic community structure: a regional analysis of streamflow patterns. Can. J. Fish. Aquat. Sci. 46, 1805–1818, http://dx.doi.org/10.1139/f89-228.

Poff, N.L., Allan, J.D., Bain, M.B., Karr, J.R., Prestegaard, K.L., Richter, B.D., Sparks, R.E., Stromberg, J.C., 1997. The natural flow regime. BioScience 47, 769–784, http://dx.doi.org/10.2307/1313099.

Puckridge, J.T., Sheldon, F., Walker, K.F., Boulton, A.J., 1998. Flow variability and the ecology of large rivers. Mar. Freshwater Res. 49, 55–72, http://dx.doi.org/10.1071/MF94161.

R Development Core Team, 2014. R: A Language and Environment for Statistical Computing, Version 3.1.0. R Found. for Stat. Comput., Vienna, Available at: http://www.R-project.org

Resh, V.H., Brown, A.V., Covich, A.P., Gurtz, M.E., Li, H.W., Minshall, G.W., Reice, S.R., Sheldon, A.L., Wallace, J.B., Wissmar, R.C., 1988. The role of disturbance in stream ecology. J. N. Am. Benthol. Soc. 7, 433–455, http://dx.doi.org/10.2307/1467300.

Richardson, A.D., Anderson, R.S., Arain, M.A., Barr, A.G., Bohrer, G., Chen, G., Chen, J.M., Ciais, P., Davis, K.J., Desai, A.R., Dietze, M.C., Dragoni, D., Garrity, S.R., Gough, C.M., Grant, R., Hollinger, D.Y., Margolis, H.A., McCaughey, H., Migliavacca, M., Monson, R.K., Munger, J.W., Poulter, B., Raczka, B.M., Ricciuto, D.M., Sahoo, A.K., Schaefer, K., Tian, H., Vargas, R., Verbeeck, H., Xiao, J., Xue, Y., 2012. Terrestrial biosphere models need better representation of vegetation phenology: results from the North American Carbon Program Site Synthesis. Glob. Change Biol. 18, 566–584, http://dx.doi.org/10.1111/j.1365-2486.2011.02562.x.

Richter, B.D., Baumgartner, J.V., Powell, J., Braun, D.P., 1996. A method for assessing hydrologic alteration within ecosystems. Conserv. Biol. 10, 1163–1174, http://dx.doi.org/10.1046/j.1523-1739.1996.10041163.x.

Rueth, H.M., Baron, J.S., 2002. Differences in Englemann spruce forest biogeochemistry east and west of the continental divide in Colorado, USA. Ecosystems 5, 45–57, http://dx.doi.org/10.1007/s10021-001-0054-8.

Running, S.W., Nemani, R.R., Hungerford, R.D., 1987. Extrapolation of synoptic meteorological data in mountainous terrain and its use for simulating forest evapotranspiration and photosynthesis. Can. J. For. Res. 17, 472–483, http://dx.doi.org/10.1139/x87-081.

Ryan, M.G., 1990. Growth and maintenance respiration in stems of Pinuscontorta and Piceaengelmannii. Can. J. For. Res. 20, 48–57, http://dx.doi.org/10.1139/x90-008.

Scott, D.W., 1992. Multivariate Density Estimation: Theory, Practice, and Visualization, Wiley Series in Probability and Mathematical Statistics. John Wiley, New York, pp. 327 pp.

Sheather, S.J., Jones, M.C., 1991. A reliable data-based bandwidth selection method for kernel density estimation. J. R. Stat. Soc. B: Met. 53, 683–690.

Silverman, B.W., 1986. Density Estimation for Statistics and Data Analysis, 1st ed. Chapman and Hall/CRC, Boca Raton, FL, 175 pp.

Snelder, T.H., Biggs, B.J.F., 2002. Multiscale river environment classification for water resources management. J. Am. Water Resour. Assoc. 38, 1225–1239, http://dx.doi.org/10.1111/j.1752-1688.2002.tb04344.x.

Stager, C., Thill, M.K., 2010. Climate Change in the Champlain Basin: What Natural Resource Managers can Expect and Do. Nature Conservancy LCBP Rep., Montpelier, VT.

Stephens, G.L., L'Ecuyer, T., Forbes, R., Gettlemen, A., Golaz, J.-C., Bodas-Salcedo, A., Suzuki, K., Gabriel, P., Haynes, J., 2010. Dreary state of precipitation in global models. J. Geophys. Res.-Atmos. 115 (D24211), http://dx.doi.org/10.1029/2010JD014532.

Stone, M.C., Hotchkiss, R.H., Hubbard, C.M., Fontaine, T.A., Mearns, L.O., Arnold, J.G., 2001. Impacts of climate change on Missouri River Basin water yield. J. Am. Water Resour. Assoc. 37, 1119–1129, http://dx.doi.org/10.1111/j.1752-1688.2001.tb03626.x.

Tague, C.L., Band, L.E., 2001. Evaluating explicit and implicit routing for watershed hydro-ecological models of forest hydrology at the small catchment scale. Hydrol. Process. 15, 1415–1439, http://dx.doi.org/10.1002/hyp.171.

Tague, C.L., Band, L.E., 2004. RHESSys: regional hydro-ecologic simulation system – an object-oriented approach to spa-tially distributed modeling of carbon, water, and nutrient cycling. Earth Interact. 8, 1–42, http://dx.doi.org/10.1175/1087-3562(2004)8<1:RRHSSO>2.0.CO;2.

Tague, C.L., Grant, G., Farrell, M., Choate, J., Jefferson, A., 2008. Deep groundwater mediates streamflow response to climate warming in the Oregon Cascades. Clim. Change 86, 189–210, http://dx.doi.org/10.1007/s10584-007-9294-8.

Tarboton, D.G., Bras, R.L., Rodriguez-Iturbe, I., 1991. On the extraction of channel networks from digital elevation data. Hydrol. Process. 5, 81–100, http://dx.doi.org/10.1002/hyp.3360050107.

Tarboton, D.G., Bras, R.L., Rodriguez-Iturbe, I., 1992. A physical basis for drainage density. Geomorphology 5, 59–76, http://dx.doi.org/10.1016/0169-555x(92)90058-v.

Taylor, K.E., Stouffer, R.J., Meehl, G.A., 2011. An overview of CMIP5 and the experiment design. Bull. Am. Meteorol. Soc. 93, 485–498, http://dx.doi.org/10.1175/BAMS-D-11-00094.1.

van Haren, R., van Oldenborgh, G., Lenderink, G., Collins, M., Hazeleger, W., 2013. SST and circulation trend biases cause an underestimation of European precipitation trends. Clim. Dynam. 40, 1–20, http://dx.doi.org/10.1007/s00382-012-1401-5.

Visbeck, M.H., Hurrell, J.W., Polvani, L., Cullen, H.M., 2001. The north Atlantic oscillation: past, present, and future. Proc. Natl. Acad. Sci. U. S. A. 98, 12876–12877, http://dx.doi.org/10.1073/pnas.231391598.

Warren, D.R., Robinson, J.M., Josephson, D.C., Sheldon, D.R., Kraft, C.E., 2012. Elevated summer temperatures delay spawn-ing and reduce redd construction for resident brook trout (*Salvelinus fontinalis*). Glob. Change Biol. 18, 1804–1811, http://dx.doi.org/10.1111/j.1365-2486.2012.02670.x.

White, K., Pontius, J., Schaberg, P., 2014. Remote sensing of spring phenology in northeastern forests: a comparison of methods, field metrics and sources of uncertainty. Remote Sens. Environ. 148, 97–107, http://dx.doi.org/10.1016/j.rse.2014.03.017.

White, M.A., Thornton, P.E., Running, S.W., Nemani, R.R., 2000. Parameterization and sensitivity analysis of the BIOME–BGC terrestrial ecosystem model: net primary production controls. Earth Interact. 4, 1–85, http://dx.doi.org/10.1175/1087-3562(2000)004<0003:PASAOT>2.0.CO;2.

Wigmosta, M.S., Vail, L.W., Lettenmaier, D.P., 1994. A distributed hydrology-vegetation model for complex terrain. Water Resour. Res. 30, 1665–1679, http://dx.doi.org/10.1029/94WR00436.

Wolman, M.G., Miller, J.P., 1960. Magnitude and frequency of forces in geomorphic processes. J. Geol. 68, 54–74, http://dx.doi.org/10.1086/626637.

Wuebbles, D., Meehl, G., Hayhoe, K., Karl, T.R., Kunkel, K., Santer, B., Wehner, M., Colle, B., Fischer, E.M., Fu, R., Goodman, A., Janssen, E., Kharin, V., Lee, H., Li, W., Long, L.N., Olsen, S.C., Pan, Z., Seth, A., Sheffield, J., Sun, L., 2013. CMIP5 climate model analyses: climate extremes in the United States. Bull. Am. Meteorol. Soc., http://dx.doi.org/10.1175/BAMS-D-12-00172.1.